Inelastic scattering of x-ray and synchrotron radiation in crystals, coherent effects in inelastic scattering[1)]

V. A. Bushuev and R. N. Kuz'min

Moscow State University

Usp. Fiz. Nauk 122, 81–124 (May 1977)

PACS numbers: 61.10.–i, 78.70.Ck

CONTENTS

1. INTRODUCTION

Studying the processes that occur in the scattering of electromagnetic radiation gives us highly extensive information on the structure and properties of matter. The scope and nature of this information depends substantially on the range of wavelengths of the radiation used and the region of the frequency-angle spectrum in which one makes the observation.

As we know, two types of scattering are distinguished in accord with the frequency criterion: elastic, in which the frequency of the scattered waves equals the frequency of the primary radiation, and inelastic scattering, i.e., that which involves a frequency shift. These types are also referred to as "coherent" and "incoherent" scattering, though we shall use these terms henceforth to denote spatial coherence in scattering.

X-ray scattering is a widespread and useful method for studying many properties of matter. As is well known, considerable advances have been made in deciphering the spatial structure of crystals and biological molecules by using x-ray diffraction, which amounts to elastic coherent, i.e., Bragg scattering.

This review is concerned with studying inelastic scattering in the x-ray wavelength range ($\lambda \sim 0.1$–10 Å), where interest has arisen in the past decade in connection with the creation of sufficiently powerful x-ray sources. In contrast to elastic scattering, inelastic scattering (IS) permits one to determine the momentum-energy "structure" of matter. The frequency change in inelastic scattering directly corresponds to the participation of some sort of elementary excitations in the scattering process. Depending on the nature of these excitations and the conditions of experiment, inelastic x-ray scattering can be either incoherent or coherent.

Let ω_1, $\mathbf{k}_1$, $\mathbf{e}_1$, and ω_2, $\mathbf{k}_2$, $\mathbf{e}_2$ be respectively the frequency, wave vector, and polarization of the incident and the scattered radiation; then the quantities $\omega = \omega_1 - \omega_2$ and $\mathbf{k} = \mathbf{k}_1 - \mathbf{k}_2$ determine the energy and momentum imparted to the medium in the elementary scattering event. One can smoothly vary the imparted momentum over a broad range by a simple change in the observation angle ϑ, i.e., the angle between $\mathbf{k}_1$ and $\mathbf{k}_2$, by studying for each fixed ϑ the frequency and polarization distribution of the scattered radiation.

While the straight line $\omega_2(\vartheta) = \text{const} = \omega_1$ corresponds to elastic scattering in the frequency-angle $\omega\vartheta$ spectrum, the frequency-angle spectrum covers an entire region in the case of inelastic scattering. The importance of studying inelastic scattering is explained by the fact that one can get considerable information on the nature of the equilibrium $\omega\mathbf{k}$ spectrum of the material from the shape of the experimentally observed frequency-angle scattering spectrum.

In the optical range, which has been best studied up to now, the $\omega\mathbf{k}$ region is limited to frequencies ω of the order of 3×10^{15} sec^{-1} (energies ~ 2 eV) and quasimomenta k of the order of 10^5 cm^{-1}. Moreover, one usually has to restrict the treatment only to optically transparent media. Yet many elementary excitations of interest in solids have energies from units to several tens and thousands of electron volts, while their quasimomenta extend to the boundaries of the Brillouin zone ($\sim 10^8$ cm^{-1}). Evidently one can encompass this range of energies and momenta only by using inelastic scattering of relatively hard and penetrating x rays.

Since no fewer than two quanta participate in an elementary inelastic-scattering event, two of which are the incident and scattered photons, inelastic scattering is by this criterion a nonlinear process. This review will treat the following forms of linear spontaneous inelastic x-ray scattering: Compton, plasmon, Raman, and parametric scattering. The term "linear" denotes that the intensity of the scattered waves is proportional to the

[1)]An abbreviated text of the review was given at the session of the seminar on synchrotron radiation in the Institute of Physical Problems of the Academy of Sciences of the USSR on June 27, 1975.

first power of the intensity of the radiation incident on the medium, while "spontaneous" means that this intensity is insufficient for the onset of superlinear (e.g., exponential) growth of the scattered intensity. This assumption holds with much room to spare for all existing x-ray sources.

Insofar as we know, this study is the first and rather complete review on the four types of inelastic x-ray scattering listed above. The review briefly throws light on the methods of theoretical description of the stated types of inelastic scattering, the methods of observation, and the fundamental experimental results, as well as the nature of the information obtained and its interpretation; a phenomenological approach is developed for describing inelastic x-ray scattering, and attention is paid to the possible manifestation of coherent effects in inelastic scattering.

The successful development of optical studies has been considerably stimulated by the invention of powerful light sources: lasers. Just as in optics, the further progress of studies in inelastic x-ray scattering hinges to a considerable extent on the existence of powerful x-ray sources. Until recently, people exclusively used x-ray tubes and radioactive preparations for this. Evidently, synchrotron radiation in the x-ray range will find widespread application in studies of these types, owing to its high spectral intensity. Apparently this field of science will reach its full development with the appearance of short-wave analogs of the laser: x-ray and gamma lasers, and the same intensive growth of studies will happen in x-ray optics, which is going through its seventh decade, as happened in the optics of the visible with the discovery of lasers. As yet, inelastic scattering is applied mainly for spectroscopic purposes, but apparently we can speak also of later use of inelastic scattering for shifting the frequency of powerful x rays.

2. THE COMPTON EFFECT AND THE MOMENTUM DISTRIBUTION OF ELECTRONS

Compton scattering, or the Compton effect (CE) is one of the first and most widely studied forms of inelastic scattering. There are currently more than three hundred publications on this topic. Therefore we shall take up only the fundamental principles of studying the momentum distribution of electrons in matter by using Compton scattering. One can find a more detailed presentation of these problems in the earlier review by Du Mond[1] (1933) and in the relatively recent review by Cooper[2] (1971).

The Compton effect is taken to mean the scattering of hard radiation by the electrons of matter that involves an increase in wavelength, with a shift that depends on the scattering angle but not on the material of the specimen. This form of inelastic scattering was first studied in 1920 by Gray.[3] Compton[4] found a shift in wavelength upon scattering of Mo$K\alpha$ radiation in graphite, and Debye[5] and he independently explained this phenomenon by starting with a treatment of the laws of conservation of energy and momentum in the interaction of a quantum with a free electron at rest. The change in wavelength should amount to $2\lambda_C \sin^2(\vartheta/2)$, where $\lambda_C = 2\pi\hbar/mc = 0.02426$ Å is the Compton wavelength, and ϑ is the scattering angle. This was soon confirmed experimentally rather accurately.[6]

Evidently scattering of monochromatic radiation by electrons at rest should lead to a δ-function Compton spectrum. However, it was subsequently found[7] that the Compton spectral line is broader than one would have expected from taking account of nonmonochromaticity and of the divergence of the input radiation. Jauncey[8] and more rigorously Du Mond[9] explained this discrepancy by the effect of the initial momentum distribution of the electrons, which had not previously been taken into account. Actually, if ω_1, $\mathbf{k}_1$, and ω_2, $\mathbf{k}_2$ are respectively the frequencies and wave vectors of the incident and scattered radiations,[2)] the conservation laws in the nonrelativistic approximation ($\hbar\omega_1 \ll mc^2$) appear as follows:

$$\begin{aligned} \mathbf{k} &\equiv \mathbf{k}_1 - \mathbf{k}_2 = \hbar^{-1}(\mathbf{p}_2 - \mathbf{p}_1), \\ \omega &\equiv \omega_1 - \omega_2 = \frac{1}{2m\hbar}(p_2^2 - p_1^2), \end{aligned} \tag{2.1}$$

where $\mathbf{p}_1$ and $\mathbf{p}_2$ are the momenta of the electron before and after scattering. According to (2.1),

$$\omega(\mathbf{k}) = \frac{\hbar k^2}{2m} + \frac{\mathbf{k}\mathbf{p}_1}{m}. \tag{2.2}$$

The energy shift of the Compton line is given by the first term in (2.2) while the second term describes the Doppler broadening of the line as determined by the projection q of the momentum $\mathbf{p}_1$ on the axis $\mathbf{k}$. Since $k_1 = \omega_1/c = 2\pi/\lambda_1$ and $k = 2k_1 \sin(\vartheta/2)$, Eq. (2.2) implies the well-known Compton relationship for the position of the center of the Compton line for free, noninteracting electrons:

$$\omega_{20} = \omega_1\left(1 - \frac{2\hbar\omega_1}{mc^2}\sin^2\frac{\vartheta}{2}\right), \tag{2.3}$$

where ϑ is the scattering angle (the angle between the directions $\mathbf{k}_2$ and $\mathbf{k}_1$).

Evidently the spectral intensity of the line is determined by the probability of finding electrons in states having the value of the projection q that corresponds to the frequency ω given by (2.2).[9] Thus the Compton frequency profile bears information on the one-dimensional (projected on $\mathbf{k}$) momentum-distribution function of the electrons. Precisely this fact defines the importance of studying the Compton effect, since one can get the electron-density distribution $|\psi_i(\mathbf{r})|^2$ from the momentum distribution by Fourier transformation. Even the early studies of Du Mond and his associates[10] demonstrated the promise of this method in studying the electron momentum distribution, which has recently been considerably refined and reduced to a working method in many research centers.

Progress in studying the momentum distribution of the

[2)] Following the widely adopted terminology, we shall henceforth term the incident and the scattered radiation the pump and the signal.

electrons in solids, liquids, and gases has arisen mainly from two factors. First of all it has arisen from improvement in experimental technique. Second, certain simplifications in the theory of the Compton effect have permitted people rather simply and reliably to correlate the observed Compton spectra with the distribution function of the electrons of the material. The fundamental approximation in the theory of the Compton effect is the so-called momentum approximation. As will be shown below, the latter has a rather simple and pictorial physical interpretation.

A. Theory of the Compton effect. The impulse approximation

As is well known, if the electrons of a material interact with radiation of high enough frequency, such as x rays or gamma rays, then these electrons can be treated as though practically free. Such an approximation holds if the energy of the electromagnetic quantum is much larger than the binding energy of an electron in the atom. Evidently we must also require for Compton scattering that the energy and momentum imparted to the electron in the inelastic-scattering process considerably exceed its initial energy and momentum. Then we can write the conservation laws approximately in the form (2.1). Yet the effect of binding is manifested only in the fact that the atomic electrons before collision with the quanta have an initial inhomogeneous distribution having the unperturbed wave function $\psi_i(\mathbf{r})$.

The probability of transition of the "electron plus field" system from the initial state $|i, \mathbf{k}_1\rangle$ to the final state $|f, \mathbf{k}_2\rangle$ is determined by the "golden rule" of quantum mechanics[11] by using the Hamiltonian $\mathcal{H} = \mathbf{p}^2/2m + V(\mathbf{r}) + \mathcal{H}_1 + \mathcal{H}_2$. Here $\mathcal{H}_1 \sim \mathbf{p}\cdot\mathbf{A}$ and $\mathcal{H}_2 \sim \mathbf{A}^2$ are the perturbations that are linear and quadratic with respect to the vector potential $\mathbf{A}$. Since the scattering is a second-order process, i.e., it involves two photons, the $\mathbf{A}^2$ perturbation must be taken into account in the first order, and the $\mathbf{p}\cdot\mathbf{A}$ perturbation in the second order of perturbation theory. The $\mathbf{A}^2$ interaction leads to "annihilation" of the incident photon and creation of the scattered photon. Simultaneously it leads to formation of a hole in the corresponding electron shell and an excited electron in the conduction band. Strictly speaking, this recoil electron is weakly bound in the sense that its wave function is modulated by the periodic potential of the ions in the crystal. The $\mathbf{p}\cdot\mathbf{A}$ perturbation is appreciable only when the energy of the incident photon is close to the binding energy of the electron. In this case, the inelastic scattering is resonance Raman scattering, and it will be treated in Sec. 4.

In the very simple case in which the energy $\hbar\omega_1$ is much larger than the binding energy, the differential Compton-scattering cross-section for an N-electron atom as determined by the $\mathbf{A}^2$ interaction has the following form:

$$\sigma(\omega, \vartheta) = \sigma_T \frac{\omega_2}{\omega_1} \sum_{i=1}^{N} \int d\mathbf{p} |\chi_i(\mathbf{p})|^2 \delta\left(\omega - \frac{\hbar k^2}{2m} - \frac{\mathbf{kp}}{m} - \frac{\mathbf{p}^2}{2m\hbar} - \Omega_i\right). \quad (2.4)$$

Here $\sigma_T = r_0^2(\mathbf{e}_1\cdot\mathbf{e}_2)^2$ is the Thomson scattering cross-section, $r_0 = e^2/mc^2$ is the classical radius of the electron, $\mathbf{e}_1$ and $\mathbf{e}_2$ are the polarization unit vectors of the pump and the signal, respectively; $\chi_i(\mathbf{p})$ is a Fourier component of the wave function of the ground state $\psi_i(\mathbf{r})$, and $E_i = -\hbar\Omega_i$ is the binding energy of the one-electron orbital. We assume that the electron in the scattering process enters a state in the continuous spectrum having a wave function in the form of a plane wave.

Now we assume that in (2.4) we can neglect the binding energy as compared with the energy transfer $\hbar\omega$, while the momentum transfer $\hbar k$ is much greater than $p \approx \hbar/a$. That is, $ka \gg 1$, where a is the radius of the orbital. This is the impulse approximation (IA),[12-14] which has been widely applied for calculating the profiles of Compton lines. For example, in scattering of MoK_α radiation (17.4 keV) in beryllium (bonding energy of a K electron 112 eV, radius $a = 0.14$ Å) at a 170° angle, the energy transfer is $\hbar\omega \approx 1160$ eV. That is, $\Omega_i/\omega \sim 0.1$, while the parameter ka is ≈ 2.5. Evidently, within the framework of the impulse approximation, the δ-function in (2.4) implies the ordinary Compton formula (2.2) for scattering by free electrons. If the energy of the pump quantum is much greater than the binding energy, then the $\mathbf{A}^2$ term makes the major contribution,[14] as is confirmed, e.g., by studying the polarization of Compton quanta.[15]

Usually the relationship (2.4) with allowance for the impulse approximation is presented in another simpler and generally accepted form. The projection of the momentum $q = (m\omega/k) - (\hbar k/2) = (m/k)(\omega_{20} - \omega_2) = mcl/2\lambda_1 \times \sin(\vartheta/2)$ characterizes the deviation $l = \lambda_2 - \lambda_{20}$ of the signal wavelength λ_2 from the center of the Compton line $\lambda_{20} = \lambda_1 + 2\lambda_C \sin^2(\vartheta/2)$. After integration in (2.4) in the case of an isotropic distribution,

$$\sigma(\omega, \vartheta) = \sigma_T \left(\frac{\omega_2}{\omega_1}\right) \frac{m}{k} J(q), \quad J(q) = \sum_{i=1}^{N} J_i(q),$$
$$J_i(q) = 2\pi \int_{|q|}^{\infty} |\chi_i(p)|^2 p\, dp = \frac{1}{2} \int_{|q|}^{\infty} p^{-1} I_i(p)\, dp, \quad (2.5)$$

Here $I_i = 4\pi|\chi_i|^2 p^2$ is the radial density of the momentum distribution. The function $J(q)$ is called the Compton profile (CP)[9,16-18] and (2.5) is the fundamental relationship of the impulse-approximation theory. Measurement of the Compton profile with use of the following normalization per electron[16,18]:

$$\int_{-\infty}^{\infty} J_i(q)\, dq = \int_{0}^{\infty} I_i(p)\, dp = 1 \quad (2.6)$$

permits us to determine the probability of finding an electron with the momentum p:

$$|\chi_i(p)|^2 = \left|\frac{1}{2\pi q} \frac{dJ_i}{dq}\right|. \quad (2.7)$$

Yet usually one uses the reverse procedure in practice. That is, one first chooses a system of wave functions ψ_i, finds the theoretical value of $J(q)$, and compares it with the experimental profile. In case of considerable divergence, one chooses a different system of functions, and repeats the procedure.

Strictly speaking, the relationships (2.1)–(2.3) are not applicable to bound electrons, as was noted even by Compton[19] and shown experimentally by Ross and Kirkpatrick,[20] who found that the center of the Compton profile is slightly shifted with respect to (2.3) toward shorter wavelengths. Bloch[21] and later Eisenberger and Platzman[14] and Currat and his associates[22,23] showed that this is due to the effect of the "parent" atom (or more exactly, ion) on the wave function of the recoil electron, which can no longer be considered to be a plane wave.[3)] However, in the impulse approximation, i.e., with large enough energy and momentum transfers, one can consider the atomic electrons to be free in the kinematic sense. Hence, one must measure the Compton profile with harder radiation and at larger scattering angles in order to improve the accuracy. Actually the potential V in the Hamiltonian $\mathcal{H}$ is not negligibly small—it leads to the inhomogeneous distribution of $\psi_i(\mathbf{r})$—but the time of interaction in the scattering process is so short that the position of the electron here hardly varies, and the potential energy after collision with the quantum is the same as before collision.[14]

The impulse approximation for electrons of the ith type is not applicable in the frequency region $\omega \sim \Omega_i$. The inelastic-scattering intensity in the range $\omega = 0$ to Ω_i is zero, and the Compton profile is not symmetrical. A sharp jump at $\omega = \Omega_i$ in the Compton profile of graphite and diamond has been observed, e.g., by Cooper and Leak.[27] The width of the forbidden band plays the role of the binding energy in scattering by the valence electrons of an insulator.[28] It is more correct[22,23,29,30] to normalize the overall Compton profile not to Z, as in (2.6), but to the Waller–Hartree expression (see, e.g., Ref. 31):

$$Z - \sum_{ij} |f_{ij}(\mathbf{k})|^2, \quad \text{where} \quad f_{ij}(\mathbf{k}) = \int \psi_i^*(\mathbf{r})\,\psi_j(\mathbf{r}) \exp(i\mathbf{k}\mathbf{r})\,d\mathbf{r}.$$

A detailed analysis of the theory of the impulse approximation is given in the ground-breaking studies of Platzman, Tzoar, and Eisenberger[13,14] and of Currat *et al.*[22,23] In spite of these substantial simplifications, the impulse approximation gives striking accuracy in describing the profile of the Compton effect, and it agrees well with the results of numerous exact calculations.[2] An evident advantage of this approximation is its simplicity together with its high accuracy.

Both outer and intra-atomic electrons contribute to the Compton profile. The wave functions of the outer electrons in a solid strongly differ from the ψ-functions of the free atoms, while we can neglect overlap with neighboring atoms for the strongly bound electrons. Consequently one can calculate the contribution to the Compton profile from the localized atomic electrons with high accuracy. Hence, if we know the overall experimental profile, we can easily isolate by simple subtraction the contribution of the outer electrons, which bears information on their Bloch wave functions.

To illustrate, we present the form of the Compton profile for the example of an idealized model of the behavior of the electrons in a metal.

For a degenerate electron gas, $|\chi(p \leq p_F)|^2 = 3/4\pi p_F^3$, and $|\chi|^2 = 0$ for $p > p_F$, where $p_F = \hbar k_F$ is the Fermi momentum. Equation (2.5) implies that the Compton profile J_f of the conduction electrons has the shape of an inverted parabola[9,13]:

$$J_f(q) = \frac{3}{4p_F^3}(p_F^2 - q^2). \tag{2.8}$$

In the free-atom model having the K-electron wave function $\psi_K = (\pi a^3)^{-1/2} \exp(-r/a)$, where $a = a_0/Z$, and $a_0 = \hbar^2/mc^2$ is the Bohr radius,

$$J_K(q) = \frac{16}{3\pi} \frac{q_K^5}{(q_K^2 + q^2)^3}, \tag{2.9}$$

Here the quantity $q_K = h/a$ determines the width of the Compton profile of the K electrons. This implies that $J_K(0)/J_f(0) = (64/9\pi)k_F a$. For example, this amounts to 0.44 for lithium (the inverse relationship holds for the line widths). The profile J_f shifts to shorter wavelengths with decreasing k, while the profile of the $1s^2$ electrons differs from (2.9), since here the validity of the impulse approximation breaks down.[13,32]

Figure 1 shows the result of Phillips and Weiss[29] from observing the scattering of Mo$K_{\alpha_{1,2}}$ radiation in Li at a 117° angle (the upper curve with the dots). The lower solid curve is drawn for the K_{α_1} component corrected for background and absorption. The dotted curves 1 (inverted parabola) and 2 are calculated respectively for the free conduction electrons and for the $1s^2$ electrons in the Hartree–Fock approximation. The position of the jumps in the derivative dJ/dq determines the diameter of the Fermi sphere in the direction of the vector $\mathbf{k}$.

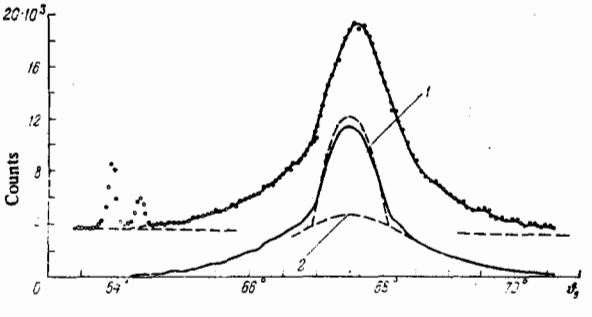

FIG. 1. Compton profile of polycrystalline lithium (lower solid curve). Curves 1 and 2 are calculated respectively for conduction electrons and $1s^2$ electrons. The angular position of the LiF analyzer crystal ((600) reflection) is plotted as the abscissa, and the number of counts per 30 min time interval is the ordinate.

[3)] Solution of the Schrödinger equation without account for the crystal potential leads to a hypergeometric function of the final state. A calculation more exact than in the impulse approximation of the scattering by a bound electron is given in Refs. 14, 21–25, and a comparison with experiment has been given[26] for N_2, O_2, and Ne that shows that the agreement improves with shorter pump wavelength.

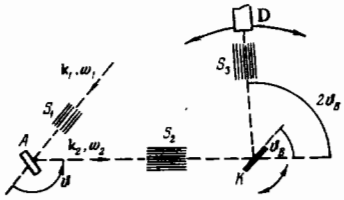

FIG. 2. Fundamental experimental scheme for studying the spectral intensity distribution of inelastic scattering of x rays. $\mathbf{k}_1$, ω_1, and $\mathbf{k}_2$, ω_2 are respectively the wave vectors and frequencies of the pump and the signal, ϑ is the scattering angle, S_1, S_2, and S_3 are collimators, A is the specimen, K is the analyzer crystal, and D is the detector having $\vartheta : 2\vartheta$ geometry.

B. Fundamental principles and results of experimental determination of Compton profiles

Figure 2 shows a typical experimental system applied for studying the spectra of all types of inelastic scattering. Upon passing the collimator S_1, the x rays strike the studied specimen A. The scattered radiation is collimated in the chosen direction, and it falls on a crystal analyzer K (generally LiF in the (400) reflection). The signal is scanned into a frequency spectrum by rocking the crystal analyzer, which plays the role of the prism in optics, through small angles (~ 5°). This happens because each energy component ω_2 corresponds to a certain Bragg angle ϑ_B, according to the Bragg law. Instead of a single crystal K, one often uses a two-crystal spectrometer to increase the resolution. Upon passing the collimator S_3, the signal is measured with a scintillation detector (usually NaI) followed by a photomultiplier and an energy discriminator. Then by supplementary fluorescence measurements, which consist in replacing the scatterer with a specimen made of the material of the anode of the tube, one finds the profile of the radiation at the undisplaced frequency (the instrumental function), and introduces the needed instrumental and theoretical corrections. The experimental inelastic-scattering profile is the convolution of the instrumental function with the true profile.

The current stage in the experimental determination of Compton profiles began in 1965 with the study by Cooper, Leak, and Weiss, [33] who observed the Compton profile of lithium. A detailed presentation of different experimental systems and correction methods can be found in Refs. 2, 22, 26–30. A method developed by Tsvetkov and Shevtsov[34] permits one to perform satisfactory studies on a commercial Soviet apparatus: the URS-60 x-ray apparatus with the BSV-2 tube, the GUR-3 goniometer, and the SSD counter unit.

One must make the following corrections for exact determination of the inelastic-scattering profile: account for the doublet structure of the radiation of the tube[35]; account for the absorption in the specimen and the analyzer, which depends on the wavelength and the experimental geometry[36]; the background correction[37]; the apparatus (divergence, nonmonochromaticity, etc.) corrections[2,38]; and the relativistic correction, [39] whose roles increase with increasing energy of the pump quanta. Multiple (mainly double) Compton scattering also distorts the intensity (~ 10%) and the shape of the true Compton profile.[40] Therefore experiments should be performed with specimens of varying thicknesses, with subsequent extrapolation of the results to zero thickness.

Before 1970, people exclusively used Mo$K\alpha$ (17.37 keV) and Ag$K\alpha$ (22.16 keV) x-ray tubes of power 2–5 kW for pumping. This permitted one to work mainly with light specimens having $Z < 15$. The counting rate here is ~ 1–100 counts/sec. X-ray tubes have nevertheless made possible an advance into the region of such elements as Sc, Ti, Mn, Fe, [41] and V and Cr.[42] It has been possible to make greater advances by using the radiation of γ-radioactive preparations of ^{241}Am (59.54 keV)[43–45] and ^{123m}Te (159 keV)[46] (with detection by Ge(Li) or Si(Li) solid-state detectors), [45] since here the photoabsorption decreases and the accuracy of the impulse approximation increases.

The theory shows that the Fermi surface is "diffuse" in metals, owing to electron-electron correlation (in Li and Na about 14% of the conduction electrons lie above the ideal sphere), and anisotropic because of the effect of the crystal lattice.[48] The electron correlation must lead to appearance of long, gently sloping tails at high $|q|$ at the base of the parabola of (2.8)[49] (see Fig. 1 at $\vartheta_B \gtrsim 68°$ and $\vartheta_B \lesssim 67°$). The Compton profile is also anisotropic in ionic crystals, [50] and account taken of the overlap of the wave functions of neighboring ions[51] leads to a difference in the intensity at the center of the line of about 10% as compared with the free-ion model. [52]

The effects of electron correlation[29,53] and anisotropy[42,43,48,53,54] can be quite reliably determined from the shape of the Compton profile as measured with different directions of the imparted momentum k. The accuracy of these experiments amounts to 1–3%, and it is continually being improved.[55] Figure 3 shows the Compton

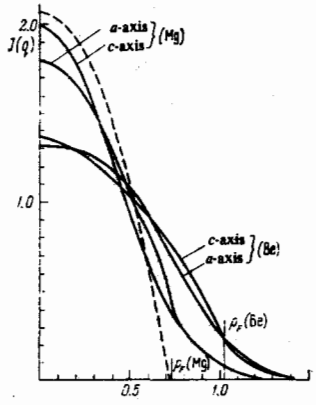

FIG. 3. Experimental Compton profiles of magnesium and beryllium normalized to the valence-electron density, as measured in the orientations $\mathbf{k} \parallel \mathbf{a}$ and $\mathbf{k} \parallel \mathbf{c}$. Pump: Mo$K\alpha$ radiation (0.71 Å), scattering angle: 155°. The dotted curve corresponds to the Compton scattering of magnesium in the degenerate electron gas model. The thin vertical lines indicate the positions of the Fermi momenta, and the projection of the momentum q is plotted as the abscissa in atomic units (1 atomic unit = 1.99×10^{-19} g · cm · sec^{-1}).

profile of the conduction electrons in magnesium and beryllium with **k** || **a** and **k** || **c** as measured by Weiss.[53] The profile for Mg in the free-electron model of (2.8) is given for comparison. One can see the sharply marked anisotropy and the presence of the tails in the momentum distribution for $p \geq p_F$.

One can also get information on the spatial distribution of the valence electrons from data on the elastic x-ray scattering intensity[31] and from experiments on electron-positron annihilation.[56] Yet the sensitivity of the atomic scattering factors to the form of the wave functions of the outer electrons is much smaller than the sensitivity of the Compton profile, owing to their considerable diffuseness. It suffices to note that the width of the Compton profile of atoms in a solid varies in some cases by more than 40% as compared with the free atoms, whereas the diffraction intensity, which is determined mainly by the inner electrons, varies only by several percent,[55] while a precise determination of the atomic factor requires laborious measurements of the absolute scattering intensity. In the case of annihilation, though the main contribution to the effect comes from the outer electrons, interpretation of the angular annihilation profile requires a knowledge of the wave function of the thermalized positron in the solid, which in itself is a complicated problem. Moreover, this method is less sensitive to the shape of the high-energy tails in the momentum distribution function of the electrons.[29]

3. SCATTERING OF X RAYS BY PLASMONS

As we noted in Sec. 2, valence and bound electrons behave similarly in the kinematic sense when the momentum transfers $\hbar\mathbf{k}$ are large enough. However, a number of interesting and important features arise in x-ray inelastic scattering with decreasing angle ϑ.

Small-angle scattering by strongly bound atomic electrons, in which the position of the spectral line is determined by the binding energy $\hbar\Omega$ ($\omega \sim \Omega$) and does not depend on the scattering angle, is commonly called Raman scattering of x rays (see Sec. 4).

Yet in the case of inelastic scattering by free valence electrons and conduction electrons, the shape of the Compton line becomes considerably distorted with decreasing **k** and its intensity declines. According to Nozières and Pines,[57] the differential inelastic-scattering cross section $\sigma(\omega, \vartheta)$ is determined by the Fourier image of the density–density correlation function for the electrons, and it can be expressed in terms of the longitudinal dielectric constant $\varepsilon(\mathbf{k}, \omega)$:

$$\sigma(\omega, \vartheta) = \sigma_T S(\mathbf{k}, \omega) = -\sigma_T \frac{\hbar k^2}{4\pi^2 e^2 n_0} \operatorname{Im} \varepsilon^{-1}(\mathbf{k}, \omega), \qquad (3.1)$$

where $S(\mathbf{k}, \omega)$ is the structure factor.

A detailed analysis of the Compton profile for a degenerate electron gas was first performed by the Japanese physicists Ohmura and Matsudaira.[58] They showed that the main contribution to the scattering cross section comes from the $\mathbf{A}^2$ perturbation in the interaction Hamiltonian. If we neglect the Coulomb interaction

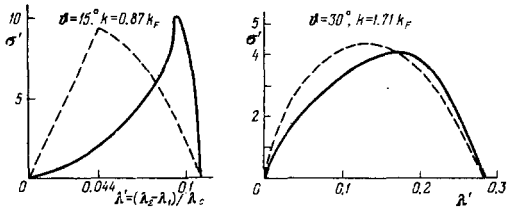

FIG. 4. Profile of the Compton line for free electrons having the density $r_s = 2$. The dotted and solid curves refer respectively to the Hartree–Fock and random-phase approximations; $\lambda_1 = 1$ Å and λ_2 are the wavelengths of the pump and the signal, λ_C is the Compton wavelength, $\sigma = \sigma(\lambda_s)\lambda_C / n_0 r_0^2$, and $k_F = (3.64/r_s)$ Å^{-1} = 1.82 Å^{-1}.

of the electrons (the Hartree–Fock approximation), which is substantial at small **k**, then the decrease in the Compton cross section and the distortion of its profile are explained[58,59] by the effect of the Pauli exclusion principle, since now only those electrons participate in Compton scattering that receive a momentum **k** sufficient to remove them from the limits of the Fermi sphere.

As we know, the Hartree–Fock (HF) approximation gives $\varepsilon^{-1}(\mathbf{k}, \omega) = 1 - 4\pi\alpha(\mathbf{k}, \omega)$, where α is the Lindhard polarizability of the electron gas,[60] and the Compton line for $k > 2k_F$ has the shape of the inverted parabola of (2.8) that is displaced from the undisplaced line in such a way that $\omega_2 \neq \omega_1$ always holds. When $k < 2k_F$, the Pauli principle comes into action, and the Compton profile consists of a parabolic region in the long-wavelength part of the spectrum and an inclined straight line in the short-wavelength part that extends as far as the pump frequency ($\omega_{2\max} = \omega_1$, $\sigma(0, \vartheta) = 0$) (Fig. 4).

When we take account of the Coulomb interaction of the electrons in the random-phase approximation (RPA),[57] we get $\varepsilon(\mathbf{k}, \omega) = 1 + 4\pi\alpha(\mathbf{k}, \omega)$. This leads to an additional suppression of one-particle excitations and to line distortion.[58] Actually in this case $\sigma^{\mathrm{RPA}}(\omega, \vartheta) = \sigma^{\mathrm{HF}}(\omega, \vartheta) |\varepsilon(\mathbf{k}, \omega)|^{-2}$. Figure 4 shows the result of calculating[58] the profile of the small-angle Compton scattering in an electron gas having the relative density $r_s = r_e/a_0 = 2$ for the angles $\vartheta = 15°$ and 30°, where a_0 is the Bohr radius, $r_e = (3/4\pi n_0)^{1/3}$ is the radius of the sphere occupied by the electron, and n_0 is the density of the valence electrons. The stated density value is close to r_s for aluminum and beryllium. Experiments in lithium[28,61,62] and beryllium[63] have fully confirmed the results of the analysis.[58]

As (3.1) implies, when $\varepsilon(\mathbf{k}, \omega) = 0$, another form of inelastic scattering is possible in small-angle scattering by free electrons in a solid. It involves excitation of longitudinal plasma oscillations, or collective fluctuations in the electron density. Plasma oscillations as an independent form of electronic excitations arise from Coulomb interaction among the electrons, and they have been widely studied in an entire set of studies (see, e.g., the monographs by Pines[64] and by Platzman and Wolff[65]). The concept of plasmons (quanta of plasma oscillations) permitted Pines and Bohm[66] to point out the connection between a fraction of the characteristic

(discrete) energy losses observed in passage of fast electrons through metallic foils and the excitation of collective oscillations. Numerous experiments on the characteristic losses of electrons have shown that, in contrast to a gaseous plasma, long-wavelength plasmas in the system of valence electrons in a broad set of metals, semiconductors, and even insulators constitute well defined elementary excitations.

Highly intensive theoretical[67] and experimental[68] studies on light scattering by low-frequency plasmons in semiconductors began with the invention of lasers.

The possible scattering of x rays with excitation of plasmons in a solid was first pointed out by Nozières and Pines[57] in 1958. The problem of small-angle inelastic scattering by the electrons of a solid-state plasma was treated in greater detail in the early period of studies[4] in the papers by Agranovich and Ginzburg[70] and by Ohmura and Matsudaira.[58] From the classical standpoint, one can interpret plasmon scattering as the inelastic scattering of x rays by the ensemble of electrons bound by Coulomb interaction, whose density has been modulated at the frequency of the plasma oscillations as a result of collective fluctuations. Just like the characteristic-loss cross-section, plasmon scattering (PS) is described by the function $\mathrm{Im}\varepsilon^{-1}$, and the equation $\varepsilon(\mathbf{k}, \omega) = 0$ determines the spectrum $\omega(\mathbf{k})$ of the longitudinal plasma waves.

Thus plasmon scattering is a combination process in which the frequency of the scattered quanta is smaller than that of the incident quanta by the frequency of the plasma oscillations. At small enough momenta k in a degenerate electron gas, the dispersion law of the plasmons looks like[64]:

$$\omega(\mathbf{k}) = \omega_p + \frac{3}{10}\frac{(v_F k)^2}{\omega_p}, \qquad (3.2)$$

Here $\omega_p = \sqrt{4\pi n_0 e^2/m}$, and $v_F = (4.22/r_s)\times 10^8$ cm/sec is the Fermi velocity. Since we have $k = 2k_1 \sin(\vartheta/2)$ to high accuracy, the spatial dispersion of the dielectric constant $\varepsilon(\mathbf{k}, \omega)$ is manifested experimentally in the dependence of the signal frequency on the angle of observation.

In the random-phase approximation, the plasmons are nondecaying excitations for k smaller than the critical wave vector $k_c = \omega_p/v_F = (1.71/\sqrt{r_s})$ Å^{-1} at which the collective spectrum of (3.2) and single-particle spectrum of (2.2) begin to overlap in the coordinates $\omega, \mathbf{k}$.[64] Owing to the Coulomb and Fermi screening of the single-particle excitations that are manifested in the inelastic-scattering spectrum as Compton scattering, the plasmons make the major contribution to the intensity of the small-angle inelastic scattering. When $k > k_c = 2k_1 \times \sin(\vartheta_c/2)$, the plasmons rapidly decay (Landau decay[71]). This must lead to a considerable broadening and disappearance of the plasmon peak. In this angular region the inelastic scattering is governed mainly by the spectrum of the individual excitations.

In the very simple case in which $\varepsilon = 1 - (\omega_p/\omega)^2$ (long-wavelength approximation), we have the following expression for the integral plasmon-scattering cross-section, as is implied by (3.1):

$$\sigma(\vartheta) = 2\sigma_T \left(\frac{\hbar\omega_1}{mc^2}\right)\frac{\omega_1}{\omega_p}\sin^2\frac{\vartheta}{2}, \qquad (3.3)$$

This agrees with the result of the semiclassical treatment.[70] For beryllium, e.g., $k_c = 1.24$ Å^{-1}. With $\mathrm{Cr}K_\beta$ ($\lambda_1 = 2.08$ Å) pumping, this corresponds to the critical scattering angle $\vartheta_c = 24°$. Since $\hbar\omega_p = 19$ eV, then for $\vartheta = 10°$, we have $\sigma_{PS}(\vartheta) = 6\times 10^{-2}\,\sigma_T$.

Priftis and his associates[72] first observed scattering of x rays by volume plasmons in 1968 in inelastic scattering of $\mathrm{Cr}K_\beta$ radiation in lithium, beryllium, and graphite at scattering angles of 5, 10, and 15°. This new form of inelastic scattering is manifested in the spectrum in the form of an extra peak that is superposed on the Rayleigh-scattering line and the Compton-scattering line, which is weak in this angular range. Apparently plasmon scattering had not been observed earlier[73] because most experiments had been performed at $\vartheta > \vartheta_c$.

Subsequently scattering of $\mathrm{Cr}K_{\alpha,\beta}$ and $\mathrm{Cu}K_{\alpha,\beta}$ x rays by plasmons in Li, Be, graphite, and Al has been studied experimentally by groups in Greece,[73–77] Japan,[78,79] the USA,[80–84] and the DDR.[85] At small ϑ one must take account of possible excitation of plasmons in the process of diffuse scattering, even in such crystals as Si and Ge.[86] On the whole, these studies showed satisfactory agreement with the conclusions of the theory,[57,58] although they also showed some discrepancies and ambiguity of the results of different experimental groups. The behavior of the electron gas in actual crystals and its interaction with radiation in the region of small and especially of intermediate ($k \sim 1 - 2k_c$) momentum transfers has proved to be far more interesting and complicated than had been assumed. Remarkably, the experiments on x-ray plasmon scattering have served as the specific impetus toward this type of studies.

Experimental study of the plasmon scattering cross-section of (3.1) is extremely useful for determining the form of the dielectric constant, and hence also for determining the validity of any particular model of the behavior of the electrons in a solid from which ε is being calculated theoretically. To quote Pines,[64] "this function is a certain simple concept that links all the theories of the electron gas in a solid." Observation of x-ray plasmon scattering permits one to determine the energy, the lifetime, and the critical wave vector of the plasmons, and also to determine the nature of the energy spectrum of the electrons in the region below the valence band and of chemical bonds.

In summarizing the results of the performed studies, we can distinguish the following fundamental features of x-ray scattering by plasmons[5]:

[4] We are not treating here the small contribution at $\omega_1 \gg \Omega$ to the scattering cross-section by atoms with formation of plasmons in "indirect" transitions[69] owing to $\mathbf{p}\cdot\mathbf{A}$ perturbations.

[5] A brief review of the early experimental studies is found in Ref. 87.

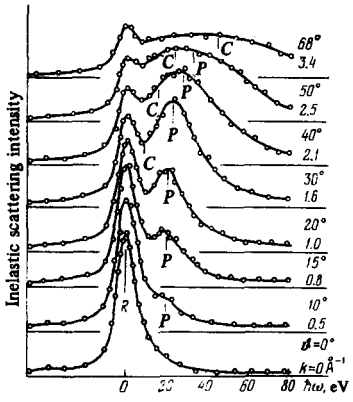

FIG. 5. Inelastic-scattering spectrum of $CrK\beta_1$ radiation (2.08 Å) in beryllium. R, C, and P indicate respectively the positions of the Rayleigh, Compton, and plasma scattering lines; $k_c = 1.24$ Å^{-1}, and $\vartheta_c = 24°$.

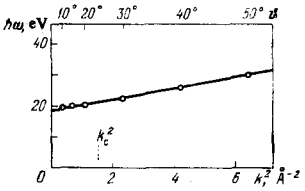

FIG. 6. Dispersion of plasmons in beryllium (pump: $CrK\beta_1$ radiation[78]).

A. Dispersion law

Figure 5 shows a typical inelastic scattering spectrum of CrK_{β_1} in beryllium for different scattering angles,[78] including those for which $k > k_c$. They found that the dispersion law of the plasmons is close to linear (3.2) with respect to k^2 (Fig. 6). Extrapolation to $k = 0$ of the position of the plasmon line gives the energy $\hbar\omega_p = 19.1$ eV. This agrees well with the theoretical value and the results on the characteristic energy losses of electrons. A dispersion law linear in k^2 has also been observed in a number of other studies.[73,79–81]

We must note that a plasmon line is also observed at momentum transfers $k > k_c$, with some exceptions,[82] though forbidden by the elementary theory. Moreover, Miliotis and Marinos[74,78] observed no appreciable plasmon dispersion dispersion in Be in the region $k \gtrsim 0.8\,k_c$, while Eisenberger *et al.* observed in lithium[83] and graphite[84] a further shift in the inelastic-scattering peak that was linear in k^2 following the horizontal region at $k \gtrsim 1.5\,k_c$ and $k \gtrsim 1.3\,k_c$, respectively. The scattering intensity at the center of the line increases with increasing ϑ, it reaches a maximum at $\vartheta \approx \vartheta_c$, and then it declines.[74]

The problem of why one observes a plasmon line at $\vartheta > \vartheta_c$ hasn't yet been solved finally at present. Yet evidently, since the conclusion of strong decay of plasmons at $k > k_c$ was made within the framework of the random-phase approximation, this theory needs further refinement and modernization. We should note that the concept itself of the critical vector, which is defined as $k_c = \omega_p/v_F$, is rather provisional.[84,88] Just as provisional is the classification at intermediate k into scattering by one-particle and collective excitations. The influence of collective effects on the inelastic-scattering spectrum holds even when $2k_F > k > k_c$. This is explained by the long-range action of the Coulomb potential $4\pi e^2/k^2$, and it is manifested in the sharp asymmetry of the spectrum of the one-particle excitations. When $k \sim 1 - 2k_c$, the latter shows peaks at the frequency $\omega \sim 1 - 2\omega_p$ that resemble the plasmon scattering line.[89]

Analysis of the first-order correction to the RPA-dielectric function shows[90] the possibility of a new scattering process in which a plasmon and an electron-hole pair are created simultaneously and satisfy the conservation law $\hbar\omega_1 + (p_1^2/2m) = \hbar\omega_2 + (p_1^2/2m) + \hbar\omega_p$. The intensity of the new peak is about 10% of the intensity of the "pure" plasmon scattering (in Be at $\vartheta = 10°$ and $\lambda_1 = 2$ Å).

As Kliewer and Raether[88] and Zacharias[91] have shown, one can explain the results of Miliotis[74] within the framework of the RPA. Following Ref. 92, one introduces into the dielectric constant of Lindhard[60] the decay of the single-electron states, and takes account of the exchange and correlation corrections on the static local field in calculating $\varepsilon(\mathbf{k}, \omega)$, as in Ref. 93.

A number of studies have established[78,81–84] that the observed plasmon dispersion is smaller than the theoretical value, and it can even be negative.[82] This cannot arise from small effects of the band structure. Platzman and Eisenberger[82,94] (see also Ref. 95) have proposed the following explanation: the sum rule[64] $\int_0^\infty \omega S(\mathbf{k}, \omega)\,d\omega = \hbar k^2/2m$ implies that if we assume that $S(\mathbf{k}, \omega) = S(\mathbf{k})\delta[\omega - \omega(\mathbf{k})]$, then $\omega(\mathbf{k}) = \hbar k^2/2mS(\mathbf{k})$. As the properties of the pair-correlation function of the degenerate electron fluid imply, the structure factor $S(\mathbf{k})$ rises from zero as k^2, reaches unity at $k \sim 1.35\,k_F$, and then performs several damped oscillations. This is necessarily reflected in the behavior of the dispersion law $\omega(\mathbf{k})$ of the plasmons.

Further refinement of the theory of the dielectric constant[93] by introducing a finite lifetime of electrons and holes has permitted[96] explanation of the existence of the gap in the inelastic-scattering spectra in beryllium, aluminum, and graphite[6)] that was observed in Ref. 95 for $k_F < k < 2k_F$. It has also permitted obtaining satisfactory agreement in Ref. 95 with the experimental data[81] on the position and shape of the plasmon line in beryllium at $k = 1.24\,k_c$.

B. Decay of plasmons

Since the conservation laws forbid conversion of a collective wave into an electron-hole pair, decay of plasmons does not exist within the framework of the random-phase approximation. This should lead to a δ-function plasmon-scattering spectral line at $k < k_c$. Precisely this conclusion was drawn in the first experiments,[79,80] owing to insufficient resolution. Yet the

[6)] The identity of the spectra in the three different substances indicates that this phenomenon arises exclusively from the properties of the electron gas, rather than from band effects. The inelastic-scattering spectrum is a superposition of a broad RPA component and a narrower plasmon peak.

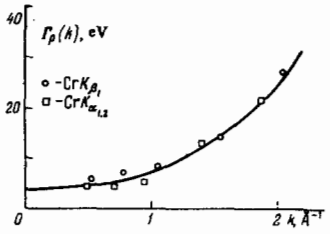

FIG. 7. Relationship of the line width (at half-height) of plasmon x-ray scattering in beryllium to the wave vector.

plasmon line has subsequently been found to have a considerable width that depends on the scattering angle.[73,74,78,81] Figure 7 shows the results of measuring[78] the width $\Gamma_p(k)$ of the line in beryllium ($\Gamma_p(0)/\omega_p = 0.2$).

One can explain the decay of long-wavelength plasmons by taking account also of such multiparticle-interaction effects as the electron–electron interactions that are forbidden in the RPA (decay of a plasmon into two electron-hole pairs, an electron-hole pair and another plasmon, etc.[97]) and, as the fundamental broadening mechanism, electron–ion interactions arising from interaction with phonons and crystal inhomogeneities.[98] At small k, we have $\Gamma_p(\mathbf{k}) = A + Bk^2$, where A and B are coefficients that depend on the model. As yet their theoretical values are still very far from the experimental values.[99] Perhaps the discrepancy involves band-structural effects. Measurement of the shape and width of the plasmon-scattering line is of importance for understanding the mechanisms of decay of plasmons.

C. Anisotropy

We have used thus far a homogeneous gas of free electrons as the model of the solid-state plasma. Actually the electrons move in the periodic potential of the crystal structure, and their wave functions are not plane waves, but Bloch waves.

The experiments in single crystals of beryllium[81] and graphite,[84] which were first performed by Eisenberger *et al.*, showed a considerable anisotropy of the plasmon-scattering cross-section. Figures 8 and 9 show the results of measuring the energy, the width, and the shape of the plasmon line in beryllium for the

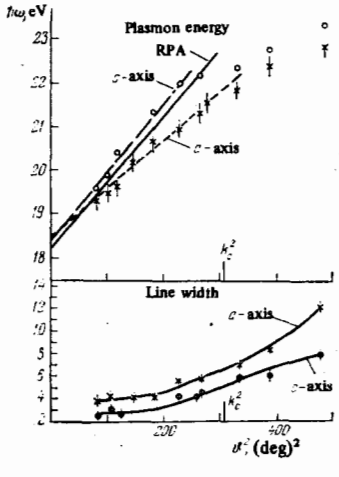

FIG. 8. Energy of plasmons in beryllium and total width of the line at half-height for the cases $\mathbf{k} \parallel \mathbf{c}$ and $\mathbf{k} \parallel \mathbf{a}$ as a function of the square of the scattering angle (pump: $CuK\alpha_1$ radiation, 1.54 Å).

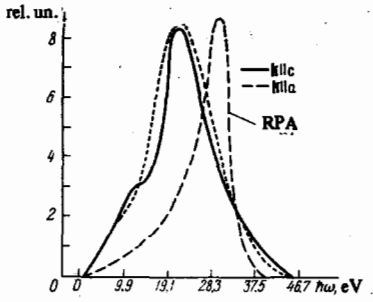

FIG. 9. Plasmon scattering spectrum of $CuK\alpha_1$ radiation in beryllium at 22° scattering angle. RPA: the result is given after correction for the instrument resolution function.

cases in which the vector k is parallel to the crystallographic axes c and a, respectively. The corresponding calculated curves in the random-phase approximation are also given for comparison.

In a crystalline medium, the function $\varepsilon^{-1}(\mathbf{k}, \omega)$ in the expression (3.1) for the cross-section has the more general form[81,85,100]:

$$\varepsilon^{-1}_{\mathbf{QQ}'}(\mathbf{k}, \omega) = \left[\delta_{\mathbf{QQ}'} - \frac{4\pi e^2}{(\mathbf{q}+\mathbf{Q})^2}\alpha_{\mathbf{QQ}'}(\mathbf{q}, \omega)\right]^{-1}, \qquad (3.4)$$

Here Q and Q′ are reciprocal-lattice vectors, the vector q is defined to be in the first Brillouin zone, and $\mathbf{k} = \mathbf{q} + \mathbf{Q}$. The explicit form of the function $\alpha_{\mathbf{QQ}'}$ is given, e.g., in the monographs[64,65]. Its tensor character with respect to Q and Q′ reflects simply the fact that in the crystal a perturbation having the wave vector k elicits responses having the wave vectors k+Q. The energy bands of the plasmos are determined by the equation $\det\varepsilon_{\mathbf{QQ}'}(\mathbf{k}, \omega) = 0$, which is a generalization of the equation $\varepsilon(\mathbf{k}, \omega) = 0$ for a homogeneous medium.[85,101] The procedure for inverting the matrix of (3.4) has been treated, e.g., in Ref. 102.

The analysis of the behavior of plasmons in crystals is based on the ground-breaking studies of Ehrenreich and Cohen[103] and of Adler and of Wiser.[102] Band calculations have been made for the real and imaginary components of ε, and also for $\mathrm{Im}\varepsilon^{-1}$, in the crystals Si,[104] Ge, GaAs and ZnSe,[105] and K and Na[106] for different crystallographic directions. They have permitted people to reveal clearly the contrast with the free-electron case and to trace pictorially the transformation of the structure factor $S(\mathbf{k}, \omega)$ with varying wave vector k.

The behavior of the tensor $\alpha_{\mathbf{QQ}'}$ depends on the details of the band structure, and it can be rather complicated. In the random-phase approximation, one must replace the function α in (3.4) by the function α_0 for a gas of noninteracting Bloch electrons. In order to understand qualitatively the results of the experiments,[81] it suffices to estimate the function $\alpha^0_{\mathbf{QQ}'}$ at the frequency $\omega \approx \omega_p$. Actually, for simple metals (Na, K, Be, Mg, Al, etc.) and certain semiconductors (Si, Ge, etc.), ω_p is large in comparison with the characteristic energies of the band structure, and the form of $\alpha^0_{\mathbf{QQ}'}$ is considerably simplified, since one can expand this tensor in powers of $1/\omega_p$. As has been shown,[81,100] account taken of the

crystalline nature of the medium, i.e., of the interband transitions in the diagonal polarizability $\alpha^0_{\mathbf{QQ}'}$ leads to a certain shift in the plasmon frequency as $\mathbf{k} \to 0$. This shift depends on the direction of the wave vector of the plasmons with respect to the crystallographic axes, and also with respect to the anisotropic character of the $\mathbf{k}^2$-dispersion of the plasmons. For a more detailed acquaintance with the influence of band-structure effects on the behavior of plasma oscillations in a solid, we can recommend referring to the monographs[84,85] and the references cited there.

A nondiagonal term characterizes coupling of the density fluctuations with the wave vectors $\mathbf{q}$ and $\mathbf{q}+\mathbf{Q}$, and it leads to existence of higher, weakly decaying plasmon bands, even with $k > k_c$, as perhaps were observed in Ref. 85.

As has been predicted in a model of one-dimensional periodicity,[107] the effects of the band structure can also lead to an energy gap in the spectrum of single-particle excitations, in which an additional low-energy collective mode exists at intermediate $\mathbf{k}$. The existence of this mode has not yet been fully confirmed experimentally.[85]

D. Temperature dependence

Upon observing the inelastic scattering of CrK_β radiation in lithium at $T = 300°$ and 77 °K, Priftis[75] found that the cross section for x-ray plasmon scattering at liquid-nitrogen temperature is about 25% smaller than at room temperature, in contrast to the case of electron excitation of plasmons, where the intensity of the energy-loss line does not depend on T. The existing theories do not explain the temperature-dependence of the plasmon-scattering cross section. One must apparently take account of photon–phonon–plasmon interaction.

E. Local plasmons

In addition to the bulk plasma oscillations in homogeneous media that we have discussed above, collective excitations can occur (local plasma oscillations[106a]) in bounded and inhomogeneous systems. An example of such systems is the electron-hole droplets in semiconductors, small metal and semiconductor particles implanted into a different medium; gas cavities produced in metals by radiation, etc. The inhomogeneous systems whose spectrum of excitations possesses collective levels as well as single-particle levels include also the electron shells of heavy atoms.

Raman scattering of light or x rays by local plasmons[106a] permits one to study the spectrum of normal vibrations of these systems. The frequencies and damping of the collective modes in an inhomogeneous electron plasma are determined by a condition more general than $\varepsilon(\mathbf{k}, \omega) = 0$, namely $\int \hat{\varepsilon}(\mathbf{r}, \mathbf{r}', \omega) n_e(\mathbf{r}')\, d\mathbf{r}' = 0$, where $n_e(\mathbf{r})$ is the effective charge density. For example, for a spherical metallic particle placed in a medium having the dielectric constant ε_1, the frequencies of the local plasmons are determined by the relationship $\omega_l = \omega_p \sqrt{l/[l+(l+1)\varepsilon_1]}$, where the l are positive integers, and $\varepsilon(\omega) = 1 - (\omega_p/\omega)^2$ for the material of the particle.

X-ray scattering with excitation of the lowest mode ($l = 1$) of the surface plasmons in small (~ 100 Å) particles of graphite and silver has been observed in Ref. 77 and has been studied theoretically in Ref. 108. Such experiments permit one to determine the limits of validity of introducing the concept of local plasmons as well defined elementary excitations, i.e., excitations having a small ratio of damping to frequency. Actually, the momentum ceases to be a well defined quantum number in inhomogeneous systems owing to scattering by the inhomogeneities. Therefore, in contrast to the RPA, a plasmon can disintegrate into an electron-hole pair even when $k < k_c$ (for more details see Ref. 108a and the references cited therein).

4. RAMAN SCATTERING OF X RAYS

Smekal[109] first pointed out in 1923 the possibility of Raman scattering (RS) of x rays by bound atomic electrons. Independently, in a study devoted to Raman scattering in the optical region, Raman[110] noted that this effect might also be manifested in the x-ray range. Subsequently electronic Raman scattering of x rays[7)] was observed in the scattering of MoK_α radiation in graphite,[111–114] aluminum,[113] and beryllium[9,113,114] in the form of narrow lines shifted downward in frequency from the position of the Rayleigh peak by about the ionization energy of the K and L electrons. The spectral width of the observed lines is close to the width of the MoK_α radiation, and the position of the lines practically did not depend on the scattering angle for $\vartheta \sim 90–160°$. The conclusion has been drawn from these results that the electron is "ejected" from the atom with zero velocity in Raman scattering. In later years, x-ray Raman scattering has been observed by Das Gupta,[115–117] Suzuki,[118] and by Faessler and Mühle[119] in the form of weak peaks on the background of the broad and intense Compton profile that arises from scattering by the outer weakly-bound electrons.

Yet we must note that these early studies were performed at the limit of the experimental potentialities of that time. This did not allow them to interpret the obtained results unambiguously. Thus, the stated effect was not detected in special experiments[120] set up to test the reports[112–117]; Mitchell,[113] Davis and Purks,[114] and Das Gupta[117] have also reported observing Raman scattering in the anti-Stokes region ($\omega_2 > \omega_1$), which was clearly impossible under the conditions of their experiments.

Inelastic scattering by bound electrons has been treated theoretically by Wentzel,[24] Bloch,[21] Sommerfeld,[121] Platzman and Tzoar,[13] and more fully in 1967 by the Japanese physicists Mizuno and Ohmura.[122] The

---

[7)] Inelastic scattering by the thermal vibrations of atoms without change in the electronic state in optics leads to Raman scattering by optical phonons and to Mandel'shtan–Brillouin scattering by acoustic phonons. In the x-ray range, the fundamental contribution to the scattering intensity comes from the acoustic vibrations, and this form of inelastic scattering is commonly called thermal diffuse scattering.[31]

law of conservation of energy for the Raman scattering process has the form

$$\hbar\omega_1 = \hbar\omega_2 + \mathscr{E} + \frac{1}{2}mv^2, \tag{4.1}$$

Here $\mathscr{E} = \hbar\Omega$ is the binding energy of the electron, $mv^2/2$ is the kinetic energy of the "ejected" atomic electron, and we assume that we can neglect the recoil energy of the atom and the excitation of lattice vibrations. The maximum energy $\hbar\omega_2 = \hbar\omega_1 - \mathscr{E}$ of the scattered quanta (the edge of the Raman line, or threshold) corresponds to the velocity $v = 0$. Sommerfeld did not account for the spreading of the atomic levels in a solid into broad, overlapping bands. Hence he found that the Raman spectrum should consist of narrow lines that correspond to transitions of the inner electrons to the unfilled outer levels of the atom. Yet Wentzel and Bloch treated scattering having large momentum transfers with transition of an atomic electron into the continuous spectrum, which corresponds more to a Compton effect involving the bound electrons, while the calculations of Platzman and Tzoar corresponded to the Compton effect in the momentum approximation and to the intermediate region between the case of large-angle scattering and that of small-angle Raman scattering.

Following Ref. 122, let us examine a Raman-scattering process in which the energy imparted to an atomic electron does not greatly exceed its ionization energy. The transition probability of the system is also determined by the "golden rule."[111] Evidently the effect of the binding of the localized electrons should be considerably manifested only at small momentum transfers $\mathbf{k}$, i.e., at relatively small scattering angles. Hence the Raman-scattering effect will be observed most clearly when the following conditions are satisfied:

$$ak = \frac{4\pi a}{\lambda_1}\sin\frac{\vartheta}{2} \ll 1, \tag{4.2}$$

$$\hbar\omega_1 \gg \mathscr{E}, \tag{4.3}$$

Here λ_1 is the pump wavelength, and a is the radius of the orbit of the electron.[8)]

When the condition (4.3), which corresponds to the case of nonresonance scattering, is satisfied, the fundamental contribution to the Raman intensity comes from the $\mathbf{A}^2$ perturbations in the interaction Hamiltonian.[114,122] When we account for (4.2) in the single-electron approximation while neglecting the effects of electron correlation, the expression for the differential Raman scattering cross-section for unpolarized radiation, e.g., by a K electron, has the following form in the non-relativistic approximation:

$$\sigma(\omega, \vartheta) = r_0^2\frac{1+\cos^2\vartheta}{2}\frac{\omega_2}{\omega_1}\mathbf{k}T(\omega)\mathbf{k}, \tag{4.4}$$

$$T(\omega_1-\omega_2) = \sum_l \langle i|\mathbf{r}|l\rangle\langle l|\mathbf{r}|i\rangle\hbar\delta(\hbar\omega_1 - \hbar\omega_2 - \mathscr{E}_i + \mathscr{E}_l),$$

$$\langle i|\mathbf{r}|l\rangle = \int \psi_i^*(\mathbf{r})\mathbf{r}\psi_l(\mathbf{r})\,d\mathbf{r}, \tag{4.5}$$

The summation in the matrix T is performed over the unoccupied states having wave functions ψ_l and energies $\mathscr{E}_l$. The expansion of $\exp(i\mathbf{k}\cdot\mathbf{r})$ in the matrix elements of T is restricted to two terms in deriving (4.4). Just as in the case of the photoelectric effect, the fundamental contribution to the Raman cross section comes from transitions to states of the continuous spectrum (in simple metals, e.g., these states lie above the Fermi level). We must average (4.5) over all orientations in scattering in polycrystals or powders. We arrive thereupon in (4.4) at the scalar product $\mathbf{k}T\mathbf{k} = t(\omega)k^2$, where $t(\omega) = (1/3)\mathrm{Sp}\hat{T}(\omega)$.

The relationships (4.2) and (4.3) explain the meaning of the term "small-angle Raman scattering." They imply that Raman scattering occurs mainly by exciting K electrons, and one must use a relatively long-wavelength pump for more reliable observation of Raman scattering. We should note that the formulated classification into Compton and Raman scattering is rather arbitrary. These are simply the limiting cases of the unitary process of inelastic scattering, in which some given part of the energy of the pump quantum is "spent" in ejecting an atomic electron.[9)] Evidently, in the case of the converse inequality to (4.2), or $ak \gg 1$, inelastic x-ray scattering goes over into the Compton effect. This is because the momentum transfer $\hbar k$ is much greater here than the momentum $p_1 \sim \hbar/a$ of the electron, and the effect of binding is small.

A qualitatively new stage in experimental study of Raman scattering of x rays started in 1967 with the studies of Suzuki and his associates[123-125] and of Alexandropoulos, Cohen, and Kuriyama,[126-129] in which they observed Raman scattering of MoK_α and CrK_α radiation in certain light substances (Li, Be, graphite, LiF, and NaCl) at different scattering angles ($\vartheta \sim 30$–$160°$). It has arisen from the invention of powerful (up to 4 kW) rotating-anode x-ray tubes and from refinement of the two-crystal spectrometer and the recording apparatus.

In summarizing the results of the studies, we can note the following fundamental characteristics of the x-ray Raman-scattering spectrum:

A. Spectral intensity distribution

The scattering spectrum is a continuous intensity distribution rather than a discrete set of lines. Here the short-wavelength edge where the intensity is a maximum lies at the threshold value of the signal frequency $\omega_2 = \omega_1 - \Omega$, and it does not depend on the scattering angle.[123,124] Figure 10 shows a typical inelastic-scattering spectrum of CrK_α radiation in boron at various angles ϑ.[124] For the K electrons of boron, $a = 0.113$ Å, and the parameter ak for scattering angles $\vartheta \sim 30$–$160°$ lies in the range 0.16–0.61, which agrees well with the requirement of (4.2).

[8)] The erroneous relationship $2\pi a/\lambda_1 \leq 1$ is found in Ref. 122 in place of (4.2), and it has been corrected later in Refs. 123 and 124.

[9)] The Raman-scattering phenomenon by localized electrons is also referred to as: "Raman effect for x rays,"[111] "fine structure in the Compton effect,"[114] "modified Smekal-Raman x-ray scattering," "Raman lines in Compton scattering,"[119] etc.

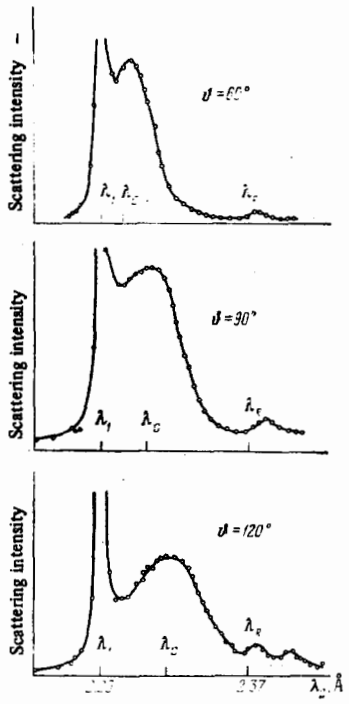

FIG. 10. Spectrum of scattering of Cr$K\alpha$ radiation (2.29 Å) in boron. λ_1, λ_C, and λ_R are the wavelengths of the peaks for Rayleigh, Compton, and Raman scattering, respectively.

The intensity of the Raman line declines smoothly toward longer wavelengths. This corresponds to a decline in the probability of transition of the electron to states of the continuous spectrum having velocities $v \neq 0$. Since the K-photoabsorption cross-section σ_ω^{ph} in the dipole approximation ($ka \ll 1$) is proportional to the expression $\omega e T(\omega) e$, where e is the polarization unit vector of the wave, $\sigma_\omega^{ph} \sim \omega t(\omega)$ in polycrystals or powders, and the shape of the Raman line for the K electrons should resemble the K absorption spectrum of soft x rays,[122,130,131] i.e., $\sigma^{RS}(\omega, \vartheta) \sim \omega^{-1}\omega_\omega^{ph}$. On the whole, this has been confirmed experimentally.[123,124,128] Figure 11 shows the inelastic-scattering spectrum of CrK_α radiation in lithium and beryllium, with the K absorption spectrum of these elements shown for comparison. Yet in the case of scattering in substances of low symmetry, there is no such simple relation between σ_ω^{ph} and $\sigma^{RS}(\omega, \vartheta)$,[130] since the photoabsorption and the Raman scattering are determined by different matrix elements (eTe and kTk, respectively). The values of the energy $\mathcal{E}$ determined in Raman-scattering experiments in Li (57 eV), Be (112 eV), B (190 eV), and graphite (284 eV)

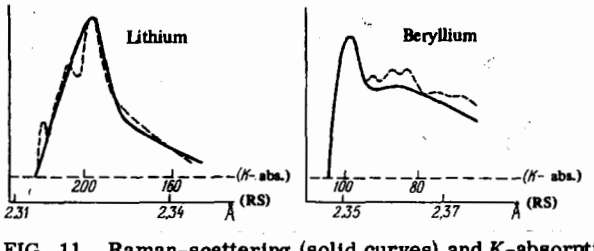

FIG. 11. Raman-scattering (solid curves) and K-absorption (dotted curves) spectra in lithium and beryllium.[124]

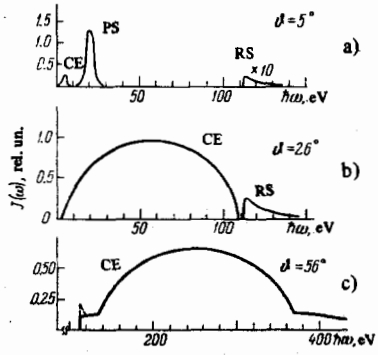

FIG. 12. Inelastic-scattering spectrum of Mo$K\alpha$ radiation (17.4 keV) in beryllium at angles of 5, 26, and 56°. CE, RS, and PS are Compton, Raman, and plasmon scattering, respectively.

agree well with the ionization energies $\mathcal{E}_K = \hbar\Omega_K$ of the K electrons as measured in x-ray absorption experiments. The position of the edge of the Raman line is sensitive to the chemical environment of the scattering atom.[132] X-ray Raman scattering has also been observed for the L electrons in Na, Al, and Si.[132]

Analysis of the fine structure of the long-wavelength edge of the Raman line combined with soft x-ray absorption experiments can give fuller information on the nature of the band structure of solids. The Raman spectrum arises from scattering practically throughout the specimen, and various inclusions and surface inhomogeneities affect its intensity but little, which can't be said of absorption spectra.

It has been shown theoretically[13,14,131] and to a certain extent experimentally[124,125,128] that the intensity of the long-wavelength tail of the Raman scattering increases with increasing scattering angle ϑ, for which the condition (4.2) ceases to hold, and the position of the Raman intensity peak ω_{20} is shifted toward smaller energies ($\omega_{20} < \omega_1 - \Omega$) to approach the Compton value.

According to (4.4), the Raman cross-section should increase with increasing scattering angle according to the law $\sigma(\vartheta) \sim (1 + \cos^2\vartheta)\sin^2(\vartheta/2)$ and decrease with increasing nuclear charge.[10] Such an angular dependence has actually been observed in scattering of CrK_β and CuK_α in Be and graphite at small angles.[125] However, the Raman intensity reached a certain maximum value with increasing ϑ, and then began to decline. One can explain this[125] by accounting for the third and fourth terms in the expansion of $\exp(i\mathbf{k}\cdot\mathbf{r})$ in the matrix elements of the transitions $|i\rangle \to |l\rangle$.

B. Line Raman scattering

In addition to transitions to states of the continuous spectrum, Raman scattering can also involve transition

[10] Babushkin[133] has obtained an angular dependence $\sim (1 + \cos^2\vartheta)/[1 + \sin^2(\vartheta/2)]^4$ resembling Compton scattering for the Raman cross section. This disagrees with the results of experiments[125] and of calculations.[122] His conclusion of a Debye–Waller dependence of the Raman cross section on the specimen temperature is also erroneous.

of an atomic electron to unfilled discrete levels. Alexandropoulos and Cohen[126] observed this form of Raman scattering in scattering of CuK_α in boron ($\mathscr{E}_K = 188$ eV) at a 60° angle in the form of lines shifted from the Rayleigh peak by 183 eV, which corresponded to the $1s \to 2p$ electronic transition. The line has a width close to that of the emission line BK_α, and it lies 5 eV above the short-wavelength edge of the broad Raman profile that corresponds to transition of $1s$ electrons to the continuous spectrum.

A rather intense, sharp Raman peak has been observed in the scattering of CuK_α radiation in lithium in the region of intermediate momentum transfers ($k/k_F \sim 1.6$–3.1). It has an energy $\hbar\omega \approx E_F = 4.7$ eV. Apparently this corresponds to the optical transition of the $2s$ electron to the upper quasi-bound $2p$ states, etc.[129] The reason why this peak is lacking at $k < k_c$[129] and at $k/k_F \sim 0.64$–2.1[83] is not yet evident.

Alexandropoulos[127] has also observed lines in the long-wavelength portion of the Raman spectrum of CuK_α and CrK_α radiations in LiF and NaCl crystals, with an energy shifted from the energy of the primary radiation by 5 eV in Lif and 2 eV in NaCl. The position and shape of these lines did not vary for angles $\vartheta \sim 16$–$84°$. This effect is interpreted as Raman scattering by F centers that are formed upon prolonged irradiation of the crystals with CuK_α x rays, and they can be used for studying the process of formation and measuring the effective masses, lifetimes, and certain other characteristics of F centers. The high intensity of the lines at a low concentration ($\sim 10^{17}$ cm^{-3}) of color centers gives evidence of the unexpectedly high cross-section of the line Raman scattering, which is an as yet unexplained fact.

Observation of inelastic scattering of the radiation from a copper tube in lithium at specimen temperatures of 300 and 77 °K has shown that the Raman intensity does not depend on the temperature, just like the cross section of the Compton effect.[134]

To generalize what we've said in Secs. 2–4, it is useful to present a schematic calculated inelastic-scattering spectrum $J(\omega)$, e.g., in beryllium ($\hbar\Omega = 112$ eV) for various scattering angles (Fig. 12). At small enough angles ϑ, the Compton effect from the conduction electrons is suppressed by Coulomb and Fermi shielding, and the plasmon scattering line (PS, see Fig. 12a) is manifested most distinctly in the spectrum. Landau damping of the plasmons occurs with increasing scattering angle, i.e., increasing momentum imparted ($k > k_c$), and the Compton line is shifted to larger ω values, while it has a parabolic line shape (see (2.8)). The Raman intensity increases, and overlap of the Compton and Raman spectra is no longer observed (Fig. 12b). This is important for a more distinct determination of their positions and shapes (a slight overlap of Compton and Raman lines in scattering of WL_{β_1} lines in beryllium at 55° angle has been observed in Ref. 32).

Figure 12c shows the scattering spectrum at a rather large angle for which $ak > 1$ and for which the condition for applicability of the impulse approximation begins to hold for the long-wavelength fraction of the scattered radiation. Here one should observe an intensity jump at the threshold frequency $\omega_2 = \omega_1 - \Omega_K$ (see, e.g., the experimental study[127]), while the inelastic-scattering spectrum is a superposition of the spectra of (2.8) and (2.9) as defined for $\omega \geq \Omega_K$ for the free and bound electrons, respectively. As we have pointed out in Chap. 2, use of harder and more penetrating radiation permits one to proceed into the region of heavier elements. Thus, steps have also been found[135] in the spectrum of γ rays of energies 412 keV (^{198}Au source, 482 keV (^{181}Hf), and 662 keV (^{137}Cs) scattered by specimens of Pd, W, and Pb, at energies lying below the initial energies by the bonding energy of the K electrons. Interaction of the recoil electron with the mother atom can lead to a singularity in the Raman profile in the vicinity of the threshold energy $\omega \sim \Omega$[131] (see the dotted curve in Fig. 12c and in Fig. 1 of the experimental study[128]). The concrete shape of this singularity depends on the shape of the wave function of the ground state and on the scattering angle.

The problem of the shape of a Raman line near the threshold is extremely important for understanding the nature of multiparticle interactions in solids. Actually, the electrons and holes that are created in the scattering process experience Coulomb interaction with one another and with other electrons and holes in the crystal. In addition, the conduction electrons interact with the ion cores, which leads to their Bloch-type behavior.

As we know, multiparticle effects can be manifested in ω-emission and absorption spectra of soft x rays near the absorption edge. These first-order processes have been studied rather broadly, both theoretically and experimentally. However, as Platzman and his associates first showed,[131] an account taken in Raman scattering of the interaction of the particles in the final states has the result that the ωk Raman spectrum near the threshold becomes far richer, and it bears valuable additional information. This is determined by the fact that the Raman cross-section depends now on the scattering angle, i.e., on the transferred momentum, as well as the frequency-dependence at fixed k.

Before we proceed to discuss the Raman scattering, let us first take up briefly the threshold features of the absorption spectra. For the sake of concreteness, we shall discuss the case of absorption in metals. In the absence of multiparticle effects, when the wave function of the photoelectron is approximated by a plane wave and the ground state is hydrogen-like, the photoabsorption cross-section is $\sigma_\omega^{ph} \sim \omega^{-3}$ for $\omega > \omega_{thr}$, and is zero for $\omega < \omega_{thr}$, where the threshold energy $\hbar\omega_{thr} = \mathscr{E} + E_F$ is the sum of the ionization energy of the corresponding electron shell and the Fermi energy. Multiparticles effects, or more precisely, Coulomb interaction between the particles, lead to a more interesting frequency-dependence of the absorption cross section near the threshold than is given by the simple one-electron theory. The manifestation of Coulomb perturbations can be provisionally classified into three parts:

1) The ejected photoelectron interacts with the hole left in the atom.

2) A rapidly produced hole can create numerous electron-hole pairs in the conduction band.

3) The ejected electron can be scattered by conduction electrons to form additional electron-hole pairs.

Only the first two effects have been analyzed in detail at present. The studies of Mahan and Nozières and their associates[11] have shown that the absorption cross section can be written in the following form with account taken of the interaction between a deep, infinitely heavy hole and the photoelectron:

$$\sigma_\omega^{ph} = \sum_l W_l(\omega) A_l(\omega), \tag{4.6}$$

where

$$A_l(\omega) = 1/[(\omega - \omega_{thr})^{\alpha_l}],$$

and

$$\alpha_l = \frac{2\delta_l}{\pi} - 2\sum_{l'}(2l'+1)\left(\frac{\delta_{l'}}{\pi}\right)^2. \tag{4.7}$$

The phase shift δ_l characterizes the scattering of the Fermi-surface conduction electrons by the hole, and the function W_l is a smooth function of the frequency. The index l characterizes the angular momentum of the initial state. The relationships (4.6) and (4.7) stem from the law of conservation of angular momentum. For example, for an s state the matrix element W_l exists only when $l=1$.

The absorption cross section of (4.6) depends very strongly on the magnitude and sign of the constant α_l. When $\alpha_l > 0$, the partial cross section increases sharply near the threshold, and it declines when $\alpha_l < 0$. An account taken of the finite lifetime of the recombining hole rules out divergence of the coefficients A_l when $\omega = \omega_{thr}$.

As has been shown, e.g., in Ref. 13, the Raman cross section is proportional to the electronic structure factor

$$S(\mathbf{k}, \omega) = (2\pi/\hbar)\sum_f |\langle f| \sum_j e^{i\mathbf{k}\mathbf{r}_j} |i\rangle|^2 \delta(\mathscr{E}_f - \mathscr{E}_i - \hbar\omega). \tag{4.8}$$

An important feature of the Raman-scattering process is that the matrix elements in Eq. (4.8) contain the complete exponential $\exp(i\mathbf{k}\cdot\mathbf{r})$ rather than the second term of its expansion, as in the one-electron dipole approximation (4.4). We recall also that a $\mathbf{k}$-dependence is generally lacking in the matrix elements for the absorption probability, since the wavelength of the radiation near the absorption edge is much larger than the dimensions of the corresponding electron orbital, the exponent kr is $\sim (\Omega/c)a \sim Z/137 \ll 1$, and we can replace the exponential by unity.

Since the factor $\mathbf{k}\cdot\mathbf{r}$ varies with the scattering angle (in contrast to the absorption case), the Raman spectrum generally contains contributions from all the powers of $\mathbf{k}\cdot\mathbf{r}$. If now, following the Mahan-Nozières theory, we take account of the Coulomb attraction between the recoil electron and the hole (central, for the sake of simplicity), and account for the mixing by the operator $\exp(i\mathbf{k}\cdot\mathbf{r})$ of the spherical harmonics of the wave function of the electron in the final state, while using the law of conservation of angular momentum, then

$$\sigma(\omega, \theta) \propto S(\mathbf{k}, \omega) = \sum_l R_l(\mathbf{k}) A_l(\omega). \tag{4.9}$$

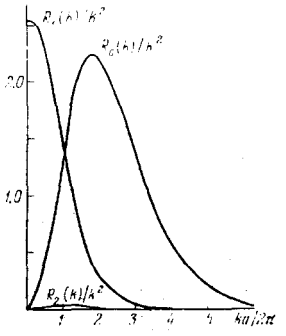

FIG. 13. Relation of the coefficients $R_l(k)$ for metallic lithium to the size of the transferred momentum in units of $2\pi/a$, where $a = 3.50$ Å is the lattice constant. The wave function of the ground state is taken in hydrogen-like form with a radius of the K shell of 0.195 Å.

The explicit form of the functions $R_l(k)$ and a graph of the first several cofactors in the case of metallic lithium are given in[131] (Fig. 13). If now we vary the scattering angle, i.e., k, then the coefficients $R_l(k)$ will vary quite significantly, and furthermore, in differing ways, depending on the index l. For example, for lithium at small k, the coefficients R_0, R_2, and the other higher terms are proportional to k^4 or higher powers, but the principal term $R_1 \sim k^2$ (cf. (4.4)). For scattering in the almost-forward direction, the threshold frequency-dependence of the Raman cross section is analogous to the cross section $W_1 A_1$ for absorption of soft x rays. The role of the coefficient R_1 declines with increasing k, and the coefficient R_0 begins to make the main contribution (the term R_2 is negligibly small). Thus the relative weights of the terms having different phase shifts are redistributed. Since $\alpha_0 = 0.41$ and $\alpha_1 = -0.1$ for lithium, the singularity near the threshold ($\alpha_0 > 0$) must be manifested for relatively large scattering angles, where the coefficient R_0 determines the main contribution. An analogous situation is reflected schematically by the dotted line in Fig. 12c. The solid curve is the scattering cross section in the one-electron approximation, toward which (4.9) approaches when $\omega \gg \omega_{thr}$.

The theory of multiparticle interactions that is developed in Ref. 131 is as yet preliminary in nature. Exact solution of the multiparticle problem faces considerable difficulties, just as in any many-body problem. Reliable experimental testing of the conclusions of the theory[131] rests in the problem of increasing the resolution, since one needs in Raman scattering an energy analysis of spectral details of characteristic dimensions of the order of 10 eV at energies of scattered quanta of the order of 10 keV.

C. Resonance Raman scattering

We have been discussing thus far the non-resonance Raman scattering of x-ray quanta having an energy much larger than the ionization energy: $\omega_1 \gg \mathscr{E}$ (we assume hereinafter that $\hbar = 1$). The theoretical and experimental study of resonance Raman scattering is yet in an embryonic state, but already the first studies have shown

[11] See Refs. 4 and 5 in Ref. 131.

the usefulness of this method for studying the spectra of deep electronic transitions.

Resonance Raman scattering, i.e., scattering of quanta having an energy $\omega_1 \approx \mathcal{E}_K$, was first observed by Sparks[136] in 1974 in the scattering of CuK_α and MoK_α radiations in Ni, Cu, Zn, Ge, and Ta in the form of lines having a sharp peak at an energy $\omega_2 \approx \omega_1 - \mathcal{E}_L$, where $\mathcal{E}_K = \hbar\Omega_K$ and $\mathcal{E}_L = \hbar\Omega_L$ are the ionization energies of the K and L electrons.[12)] The intensity of the lines declined smoothly toward lower energies. Since the energy of the pump quantum is close to the K absorption edge, the process of resonance Raman scattering must be described by $\mathbf{p}\cdot\mathbf{A}$ terms in the second-order perturbation theory. Here the L electron is "ejected" into the continuous spectrum, but not by the direct $\mathbf{A}^2$ pathway, but by a resonance pathway via an intermediate virtual K state. Actually the observed Raman intensity did not depend on the scattering angle, and it varied considerably from substance to substance, depending on the size of the mismatch $\Omega_K - \omega_1 > 0$. The measured[136] cross section for resonance Raman scattering of CuK_α radiation amounts in units of r_0^2 of from 7.0 for Ni to 1.1 for Ge.

Arguments based on considering the law of conservation of energy in scattering by the elastic and inelastic channels permitted Sparks to relate the resonance Raman-scattering intensity to the real component of the dispersion term in the atomic scattering factor, which is also described by a $\mathbf{p}\cdot\mathbf{A}$ term, and is independent of the scattering angle. However, the more rigorous direct calculation of Bannett and Freund[138] gives better agreement with experiment,[136] and it shows the incorrectness of Sparks' approach.

The phenomenon of resonance Raman scattering has been analyzed most fully in recent studies of Eisenberger, Platzman, and Winick.[139] Following the results of these studies, let us examine some features of resonance Raman scattering of x rays.[13)] Apart from insubstantial details, the electronic spectrum for simple metals is shown in Fig. 14. The lower electronic states denoted as K and L are filled. The conduction band, which is depicted in the form of a parabola, is partially filled up to the Fermi level. These levels are well resolved for most simple metals. The binding energies of the K and L electrons are of the order of thousands and hundreds of electron volts, respectively. A typical value of E_F is ~5 eV. X rays being scattered by this system can put it into various excited states, which are also well resolved.

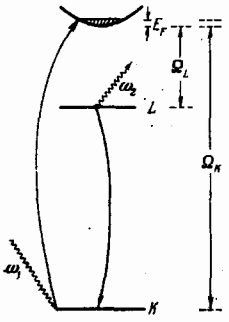

FIG. 14. Energy levels for simple metals and a diagram of electronic transitions in resonance Raman scattering.

We have already treated the phenomena that stem from an $\mathbf{A}^2$ perturbation. They are the Compton effect and plasmon scattering in the system of conduction electrons; the Compton effect within the framework of the momentum approximation and non-resonance Raman scattering by localized electrons. The $\mathbf{p}\cdot\mathbf{A}$ perturbation as accounted for in the second order leads to the following processes: the incident photon forms a hole in the K shell upon being absorbed, while ejecting the K electron into the conduction band. An electron from the L shell fills the K hole. This produces a vacancy in the L shell and gives rise to the final scattered photon.

Just as in the case of non-resonance scattering, this simple single-electron pattern actually becomes complicated by multiparticle effects, part of which have been listed above. Certain problems involving the singularity in the resonance Raman scattering near the threshold have been discussed by Nozières and Abrahams.[140] Yet if we restrict the treatment to the lower single-electron approximation, which corresponds to an experiment at low resolution, then the matrix element for this process has the form

$$M_{fi} = \frac{\langle L|\mathbf{p}\cdot\mathbf{e}_2'|K\rangle\langle k|\mathbf{p}\mathbf{e}_1|K\rangle}{m(\omega_1 - \mathcal{E}_k - \Omega_K + i\Gamma_K)}. \qquad (4.10)$$

The states $|L\rangle$ and $|K\rangle$ are bound, hydrogenlike states of the L and K electrons, $|k\rangle$ and $\mathcal{E}_k$ are the wave function and the energy of the conduction electron, and Γ_K is the phenomenological constant for radiational and radiationless decay of the K hole. This matrix element is of resonance type whenever the energy of the incident photon is higher than the threshold energy $\Omega_K + E_F$.

In this simple model, we can easily estimate the effectiveness of the contribution of the $\mathbf{p}\cdot\mathbf{A}$ perturbation as compared with the $\mathbf{A}^2$ term. If we take the $\mathbf{A}^2$ contribution to be unity, then

$$M^{\mathbf{pA}} \approx \sqrt{\frac{E_F}{\Omega_L}}\frac{\Omega_L}{\omega_1 - \mathcal{E}_k - \Omega_K + i\Gamma_K} \qquad (4.11)$$

The ratio (E_F/Ω_L) is small, yet the second resonance coefficient can more than compensate this factor if the energy ω_1 suffices to transfer the electron from the K shell beyond the Fermi surface.

In order to find the probability of resonance Raman scattering, we must as usual sum the square of the modulus of (4.10) over all the unoccupied final $\mathbf{k}$-states. Naturally, the frequency of the signal is defined by the law of conservation of energy $\omega_2 = \omega_1 - (\Omega_L + \mathcal{E}_k)$. Each

[12)] The results of Ref. 137 on observing a radiative KLL Auger effect can apparently be treated as being intra-atomic Raman scattering by the L electrons of the photons that arise in the atom itself as the K hole becomes filled by an electron from the L shell.

[13)] The fundamental problems of resonance and non-resonance Raman scattering with account for multiparticle effects have been presented rather simply and in detailed fashion in the report by Platzman and Eisenberger at the first Soviet-American symposium on the theory of light scattering in condensed media.[139]

individual photon transition can be considered to be purely dipole in type, since the wavelength of the resonance x rays is much greater than the characteristic dimensions of the electron shell. Therefore the resonance Raman cross section does not depend on the amount of momentum transferred. This feature distinguishes resonance from non-resonance Raman scattering.

Whenever the energy of the pump quantum exceeds the threshold, i.e., $\Delta\mathscr{E}_1 \equiv \omega_1 - (\Omega_K + E_F) > 0$, the real part of the denominator in (4.10) can be negligibly small, and a second-order process such as Raman scattering can be represented as absorption with emission ensuing after the time $1/\Gamma_K$:

$$W(\omega_1, \omega_2) = \Gamma_K^{-1} W^{\text{absorp}}(\omega_1) W^{\text{emiss}}(\omega_2); \qquad (4.12)$$

Here the frequency $\omega_2 = \Omega_K - \Omega_L$ does not depend on the mismatch $\Delta\mathscr{E}_1$, and it coincides with the frequency of the characteristic $K\alpha$ radiation. Thus the relationship (4.12) above the threshold describes the fluorescence spectrum.

Below the threshold, when the mismatch $\Delta\mathscr{E}_1$ is negative,

$$W(\omega_1, \omega_2) = W^{\text{absorp}}(\omega_1 - \omega_2 + \Omega_K - \Omega_L) \frac{\omega_2}{(\Omega_K - \Omega_L - \omega_2)^2 + \Gamma_K^2}. \qquad (4.13)$$

Since the absorption probability depends mainly on the process of K absorption, it varies in the energy range defined by the binding energy of the K electron. This means that the function W^{absorp} varies slowly, and it can be estimated at the threshold energy value, i.e., $W^{\text{absorp}}(\Omega_K + E_F)$. The energy-dependence of the Raman cross-section is determined mainly by the frequency denominator in (4.13).

For detailed study of resonance Raman scattering, it is very important to have a powerful x-ray source with a narrow line and a tunable emission frequency. Use of the synchrotron radiation (SR) of the SPEAR storage ring of Stanford University permitted Eisenberger, Platzman, and Winick[139] to increase substantially the pump spectral density (10^{10} photons/sec following the monochromator in an energy range of 0.9 eV, which is two orders of magnitude higher than the intensity of the characteristic lines of x-ray tubes), and to improve the resolving power of the experiment (~0.8 eV as compared with a resolution of 190 eV in Sparks' study[136]). In this study, they observed 90° resonance Raman scattering in copper near the CuK_α fluorescence line ($\Omega_K - \Omega_{L_{3/2}} = 8048$ eV). Here the energy of the pump quanta could be varied smoothly in the vicinity of the K absorption edge of copper ($\Omega_K + E_F = 8980$ eV) by rotating the silicon monochromator. This isolated from the broad SR spectrum a narrow region at some given energy. Insofar as we know, this is the first report on application of SR for studying inelastic x-ray scattering.

They confirmed experimentally that the signal frequency coincides with the fluorescent-emission frequency when $\Delta\mathscr{E}_1 > 0$. Below the threshold ($\Delta\mathscr{E}_1 < 0$), the energy of the scattered quanta declines in proportion to the increase in the negative mismatch. This experimental result agrees well with the theoretical rectilinear relationship $\omega_2 = \omega_1 - (\Omega_L + E_F)$ that is implied by (4.13), if we assume the argument of the function W^{absorp} to be equal to the threshold value $\Omega_K + E_F$.

An interesting result of Ref. 139 is that the experimental width of the Raman line with resonance pumping ($\Delta\mathscr{E}_1 = 0$) is 30% narrower than that of the fluorescent CuK_α emission that arises when the energy of the incident quanta exceeds the K absorption edge. This phenomenon can be explained[139] if one takes correct account of the finite lifetime of the K and L holes, which was neglected in the previous studies,[136,138] and which led to divergence of the Raman cross section at resonance.

Such experiments can give additional information on the various physical processes in the system and on the fine structure of the spectra near the threshold. Moreover, this method need not be restricted to transitions of the deep electrons, but can be used for studying other, more weakly bound electronic states. The success of this first experiment allows us to hope that synchrotron radiation will be widely used in the future for systematic study of inelastic x-ray scattering.

5. PARAMETRIC SCATTERING

Parametric scattering (PS) is a relatively new type of scattering. From the quantum standpoint, it is a spontaneous coherent breakdown of the pumping photons ω_1 into pairs of photons having the frequencies ω_2 and $\omega_3 = \omega_1 - \omega_2$ upon interacting with matter. This phenomenon was first observed in the optical range in 1967[141-143] in scattering of pulsed and continuous laser radiation in the non-centrosymmetric, optically nonlinear crystals KDP, ADP, and $LiNbO_3$.

Klyshko[144] made the first concrete estimate of the intensity of parametric scattering. The parametric-scattering phenomenon has been treated more fully in the studies of Klyshko,[145] Kleinman,[146] and a set of other authors.[147,148] Parametric scattering,[143] which has also been termed "parametric fluorescence,"[142,144] and "optical parametric noise"[146] is described in the third order of ordinary peturbation theory.[147] One can explain parametric scattering phenomenologically[145,146] by assuming that the medium has a nonlinear (quadratic)[14] polarizability $\hat{\beta}$. That is, the polarization is $\mathbf{P}_2 = \hat{\beta}\mathbf{E}_1\mathbf{E}_3^*$. Then the thermal (for $\hbar\omega_3 \lesssim k_B T$) and quantum fluctuations of the field $\mathbf{E}_3$ having the so-called idler or supplementary frequency ω_3 lead to the polarization $\mathbf{P}_2$ in the presence of the pump field $\mathbf{E}_1$, and hence to emission at the signal frequency $\omega_2 = \omega_1 - \omega_3$. In this approach the probability of parametric scattering is calculated in first-order perturbation theory with a perturbation energy of $\beta\mathbf{E}_1\mathbf{E}_2^*\mathbf{E}_3^*$, and parametric scattering can be correlated with Mandel'shtam–Brillouin scattering, where the equilibrium electromagnetic waves in the medium play the role of the acoustic waves.

[14] The third-order tensor $\hat{\beta}$ differs from zero only in a non-centrosymmetric medium if we neglect spatial dispersion.

In contrast to Raman scattering, the parametric-scattering spectrum does not involve directly the intrinsic frequencies of the medium, so that ω_2 and ω_3 are arbitrary in principle. The distinctive feature of this form of scattering is its coherent, directional nature of the scattering at a given frequency: scattering occurs most effectively only when the so-called spatial-synchronization condition holds for the wave vectors of the fields:

$$\mathbf{k}_1 = \mathbf{k}_2 + \mathbf{k}_3. \qquad (5.1)$$

For example, one can determine from the form of spectrum of the signal the dispersion law, the absorption coefficient, etc., of the waves at the idler frequency. Scattering is observed quite reliably when one uses the radiation of low-power (~0.1 W) gas lasers.[148] Weinberg[149] has found parametric scattering upon pumping with a mercury lamp.

Evidently the condition (5.1) can be satisfied only in the presence of anomalous dispersion, or (in a region where the material is transparent) in the presence of birefringence. This is just why parametric scattering is observed in crystals in which the anomalous dispersion is imitated by the anisotropy of the refractive index $n(\omega)$. In the x-ray range, a three-frequency interaction like (5.1) cannot be realized, since crystals are practically isotropic at x-ray frequencies, and apart from frequency regions near the photoabsorption edges, they possess a normal disperion law. That is, $n(\omega_1) > n(\omega_2)$ if $\omega_1 > \omega_2$.

Yet several methods exist for compensating the dispersion. The momentum deficit can be covered by one of the reciprocal-lattice vectors $\mathbf{Q}$ in artificial spatially-periodic (e.g., layered[150]) media having a variable refractive index or by using dielectric waveguides having a corrugated surface.[151] as are used in distributed-feedback lasers. One can also attain phase matching in a crystalline medium having a layered[152] or domain[153] structure that modulates the quadratic polarizability $\hat{\beta}(\mathbf{r}) = \sum_{\mathbf{Q}} \hat{\beta}^{(\mathbf{Q})} \exp(i\mathbf{Q}\cdot\mathbf{r})$, as well as by using an auxiliary ultrasonic pump.[154] In these cases, the synchronization condition is a nonlinear analog of Bragg's law:

$$\mathbf{k}_1 + \mathbf{Q} = \mathbf{k}_2 + \mathbf{k}_3, \qquad (5.2)$$

Here $\mathbf{Q}$ is the wave vector of the ultrasonic wave or reciprocal-lattice vector of the periodic structure.

The possibility of observing parametric scattering in the x-ray range[15] was first pointed out in a study by the the American physicists Freund and Levin[155] in 1969, where they studied lattice modulation of the quadratic polarizability of a crystal that they had brought into the synchronization condition (5.2). They showed on the basis of Kleinman's results[146] that parametric scattering can be observed by using powerful modern x-ray tubes.[16]

Since the x-ray refractive index hardly differs from unity, the synchronization condition (5.2) is satisfied only by the reciprocal-lattice nodes Q, Q', etc., that lie inside the Ewald sphere[31] of radius k_1, and the synchronization surfaces amount to ellipsoids of rotation having the axes $\mathbf{k}_1+\mathbf{Q}$, $\mathbf{k}_1+\mathbf{Q}'$, etc. These ellipsoids have one common focus at the origin of the vector $\mathbf{k}_1$, and the remaining foci at the nodes Q, Q', etc. Actually, the geometric locus of the points having the sum of distances $(\omega_2/c)+(\omega_3/c)$ from the ends of a segment of length $|\mathbf{k}_1+\mathbf{Q}| < \omega_1/c$ is an ellipsoid of rotation with its axis lying along the vector $\mathbf{k}_1+\mathbf{Q}$. Yet this requirement on the summation is nothing other than the synchronization condition (5.2).

We can write the transverse component of the polarization at the sum frequency $\omega_1 = \omega_2 + \omega_3$ in the form

$$\mathbf{P}_1^{\perp} = \beta^{(Q)\perp} E_2 E_3, \quad \beta^{(Q)\perp} = G(Q)\,\theta_{123} N_0, \qquad (5.3)$$

$$G(Q) = -i\beta_0 F(Q), \quad F(Q) = \sum_j f_j(Q) \exp(iQr_j - W_j), \qquad (5.4)$$

$$\theta_{123} = \left[\mathbf{s}_1\left[\mathbf{s}_1\left\{\frac{c}{\omega_1}(\mathbf{e}_2\mathbf{e}_3)\mathbf{Q} - \frac{c}{\omega_2}(\mathbf{e}_2\mathbf{Q})\,\mathbf{e}_3 - \frac{c}{\omega_3}(\mathbf{e}_3\mathbf{Q})\,\mathbf{e}_2\right\}\right]\right] \qquad (5.5)$$

Here $\beta^{(\mathbf{Q})\perp}$ is the transverse component of the convolution of the tensor $\hat{\beta}^{(\mathbf{Q})}$ with the wave-polarization unit vectors $\mathbf{e}_2$ and $\mathbf{e}_3$. In the free-atom model, it is defined by the so-called nonlinear structure factor $G(\mathbf{Q})$[155]; $F(\mathbf{Q})$ is the linear structure factor, f_j is the atomic scattering factor of the jth atom in the unit cell, $\exp(-W_j)$ is the Debye-Waller temperature factor[31]: $\beta_0 = e^3/m^2 c\omega_1\omega_2\omega_3$ is the quadratic correction to the polarizability of a free electron, N_0 is the cell-number density, and $\mathbf{s}_1 = \mathbf{k}_1/k_1$. We assume that the frequencies of the fields lie considerably higher than those of the K absorption edges. As the frequencies of the fields approach the absorption edges, we must take account of the complex dispersion terms in the atomic scattering factor.[156]

The integrated power (over the spectral width of the line) of the radiation scattered into a unit solid near ϑ is[155,157]:

$$P_{\vartheta} = \frac{2\pi\hbar\omega_2^3\omega_3}{c^4(1-\cos\eta)} |G(Q)|^2 \theta_{123}^2 N_0^2 S_1 V^{(e)}. \qquad (5.6)$$

Here $V^{(e)} = Al^{(e)}$ is the effective volume, S_1 and A are the pump intensity and cross-section, and $l^{(e)}$ is the effective length that accounts for the absorption of the pump and the signal. The "reflection" experimental scheme in which the signal emerges through the front face of the crystal is the most preferable for increasing the effective length.[157] Equation (5.6) implies that the parametric-scattering power increases with decreasing angle η between the scattering directions $\mathbf{k}_2$ and $\mathbf{k}_3$. Here the propagation direction $\mathbf{k}_1$ must differ slightly from the usual Bragg direction for the pump.

The following estimates[157] give a certain picture of the efficiency of paramet..ic x-ray scatterings: with a pumping power of 10^{-4} W at a wavelength of 0.71 Å (MoK_α) and with a deviation of $\mathbf{k}_1$ from the exact Bragg position by 1.5°, the counting rate in a solid angle of 0.015 sr should amount in scattering in diamond ($\mathbf{Q}$ = (400)), silicon (800), and molybdenum (400) to 144,

[15] Agranovich and Ginzburg[70] had previously treated Raman scattering of x rays with formation of excitons, which can be treated as a limiting case of parametric scattering.

[16] Strictly speaking, Kleinman's results are valid only for parametric scattering in a transparent medium. However, as Klyshko[145] has shown, the frequency-integral scattering intensity does not depend on absorption at the idler frequency, and it coincides with Kleinman's result.

9.4, and 29 quanta per minute, respectively, when $\omega_2 = \omega_3$. The effective lengths are 8×10^3, 333, and 48 μm, respectively.

Parametric x-ray scattering was observed in 1970 in a unique and as yet single experiment by Eisenberger and McCall,[158] who observed the breakdown of quanta of MoK_α radiation in beryllium into pairs of quanta of equal energy. The total power of the tube was 2 kW, the deviation of the primary beam from the Bragg direction corresponding to the $11\bar{2}0$ reciprocal-lattice direction was 15' of angle, the pump was incident at an angle of 9° to the surface of the crystal, and ϑ was 40° (a "reflection" experiment). Here they observed one signal quantum per hour in a solid angle of 2.1×10^{-3} sr on the background of a flux of Compton quanta of 2.5×10^3 sec^{-1}, which were eliminated by an energy discriminator. This agrees well with the theory. They used a coincidence system with respect to the signal and idler channels in order to reduce the noise due to the incoherent double Compton effect,[111] which consists in the scattering of a pump quantum by a free electron to yield two quanta with satisfaction of the conservation law (5.2), where the momentum of the recoil electron plays the role of **Q**.

Just as for elastic and Compton scattering, a process of incoherent two-photon scattering of the type $\omega_1 \to \omega_2 + \omega_3 = \Omega_n$ can occur with participation of real electronic transitions of excitation energy $\hbar\Omega_n$, in addition to coherent parametric scattering. The probability of this breakdown increases with increasing **Q**, and it is always smaller than the probability of the double Compton effect at a free electron.

The parametric-scattering cross section as defined by the function ϑ^2_{213} depends in a rather complicated way on the polarization of the primary and scattered radiations. Figure 15 shows the results of calculating[180] the relative intensities $\Phi_{ij} = \vartheta^2_{ikj}/(\vartheta^2_{AAA}+\vartheta^2_{ABB}+\vartheta^2_{BAB}+\vartheta^2_{BBA})$ and the degree of polarization of the signal $\rho_{AB} = (\Phi_{AA}+\Phi_{AB})/(\Phi_{BA}+\Phi_{BB})$ for the case of a coplanar arrangement of the vectors in (5.2) for an unpolarized pump. Here the subscripts A and B correspond respectively to polarizations of the fields in the scattering plane and perpendicular to it. The subscripts i, j, k take on the values A and B. The first and second subscripts in Φ_{ij} correspond to polarization of the signal and the supplementary wave, and $\Phi_{AB}(\gamma) = \Phi_{BA}(-\gamma)$. The zeros of the function Φ_{ij} can be interpreted as a nonlinear analog of Brewster's law.

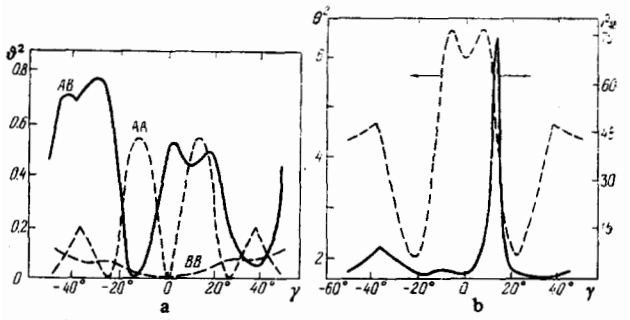

FIG. 15. Polarization characteristics of parametric scattering. a) Relative intensities $\Phi_{ij}(\gamma)$; b) degree of polarization $\rho_{AB}(\gamma)$ and the intensity $\vartheta^2(\gamma)$ averaged over the polarization states; γ is the angle between the pump vector **k** and the reciprocal-lattice vector **Q**. The curves are calculated for an unpolarized pump with a Bragg angle corresponding to $\mathbf{k}_1$ and **Q** of 39.5°.

Whenever the nodes Q are close to the surface of the Ewald sphere for the pump, the supplementary frequency ω_3 can lie in the ultraviolet or the visible. That is, processes can occur of breakdown of a pump quantum into x-ray and optical quanta[161] or of frequency addition (or subtraction) of x-ray and optical radiation.[162,163] Since $n(\omega_3) \neq 1$, the synchronization surface here near the poles of the "ellipsoids" differs from elliptical. When the nodes Q approach closer to the surface of the Ewald sphere, parametric scattering degenerates into thermal diffuse scattering, where the elastic Debye waves play the role of the supplementary waves $\mathbf{E}_3$.

The frequency shift,[162] which is also called nonlinear x-ray diffraction[161] or inelastic Bragg scattering[163] can be treated as scattering of x rays by atoms whose wave functions are perturbed by the optical-frequency field $\mathbf{E}_3(\mathbf{r}, t)$ (real or fluctuational). Here the local electron density has the form $n(\mathbf{r}, t) = n_0(\mathbf{r}) + \Delta n(\mathbf{r}, \mathbf{E}_3)$, where n_0 is the unperturbed density. Addition of the frequencies ω_2 and ω_3 leads to the polarization

$$\mathbf{P}(\omega_1 = \omega_2 + \omega_3) = -\frac{e^2}{m\omega_1^2}\mathbf{E}_2 \int \Delta n(\mathbf{r}, \mathbf{E}_3)\, e^{i\mathbf{Q}\mathbf{r}}\, d\mathbf{r}, \qquad (5.7)$$

Therefore such experiments permit one to measure the perturbation Δn directly. An essential point is that Δn is mainly determined by the structure factor of the valence electrons.[161] This is important in studying the nature of chemical bonds in matter, since one measures only the overall density $n_0(\mathbf{r})$ by using linear diffraction. They obtained encouraging estimates in Ref. 162 for performing frequency-addition experiments, which can give useful information on the states of an atom excited by light. However, attempts to mix the radiation of a nitrogen laser with an x-ray beam have as yet proved unsuccessful.[164]

In addition to the cited studies,[155–164] quantum-mechanical calculation of nonlinear polarizabilities, including also account for the contribution of the jump in electron density at the surface of the crystal, have also been performed by Jha and Woo[165] and Freund and Levin.[166] Estimates of the quadratic polarizability give the following results: $|\hat{\beta}^{(Q)}| \sim 10^{-18}(cm^3/erg)^{1/2}$ for $\lambda_1 = 1$ Å, $\omega_2 = \omega_3$, and $N_0 \sim 10^{23}$ cm^{-3}. For comparison we point out that $\beta \sim 10^{-7}$ (cm^3/erg)$^{1/2}$ for the $LiNbO_3$ crystal in the optical range. The small size of the quadratic nonlinearity at x-ray frequencies, at which the electrons of matter can be considered to be practically free, is explained in the classical approach by the smallness of the relativistic term $\propto v/c$ in the Lorentz force. Apparently the resonance polarizability of a nuclear subsystem having narrow Mössbauer transitions should be more significant. If one of the frequencies lies in the optical range ($\sim 10^{15}$ sec^{-1}), then the electronic polarizability $\beta^{(Q)}$ rises to 10^{-13} (cm^3/erg)$^{1/2}$. A calculation[165]

of the cubic polarizability has shown that the nonlinear increment $\Delta\varepsilon = -(2\pi m_0 e^4/m^3\omega_1^4 c^2)E_1^2\varepsilon$ to the linear dielectric constant ε arising from "self-action" of the wave is negative. This implies that self-focusing of x rays is impossible.

A number of studies have analyzed the possible appearance in the x-ray range of such purely nonlinear effects as two-photon emission,[167] two-quantum absorption of x-ray and laser quanta,[168] and two-quantum excitation of nuclei in oppositely-directed fluxes of γ-quanta.[169] The probability of a two-photon transition from the L to the K shell for a copper ion having a single K vacancy is of the order of 10^{-6} times the probability of a one-quantum transition, while the two-photon absorption coefficient in copper at the emission intensity of a neodymium laser of 10 MW/cm^2 must amount to several percent of the linear photoabsorption. This permits us to hope for possible experimental observation of these effects.

6. THE PHENOMENOLOGICAL APPROACH TO DESCRIBING INELASTIC SCATTERING

Two equivalent approaches can be taken for describing inelastic scattering processes. The first is concrete quantum-mechanical calculation of the scattering cross sections, and the second is phenomenological description of inelastic scattering by using concepts of the nonlinear polarizabilities of matter. This method has become most widespread in connection with the development of nonlinear optics and laser technology.[170] Evidently it is completed only by a subsequent microcalculation of the introduced polarizabilities. The method developed in the course of growth of nonlinear optics can also be extended to the region of x-ray wavelengths. This approach is a natural generalization of the linear phenomenological theory of propagation of x rays. When combined with the microapproach, it permits one to give a useful and pictorial interpretation of many inelastic-scattering phenomena, which is also of interest from the methodological standpoint.

The starting point of the phenomenological description of the electromagnetic properties of matter is the assumption that the polarization of the medium that arises under the action of the field $\mathbf{E}$ can be written in the form[170,171]:

$$\mathbf{P} = \hat{\alpha}\cdot\mathbf{E} + \hat{\beta}:\mathbf{EE} + \hat{\gamma}\vdots\mathbf{EEE} + \ldots, \tag{6.1}$$

Here $\hat{\alpha} = (\hat{\varepsilon}-1)/4\pi$, $\hat{\beta}$, and $\hat{\gamma}$ are the tensors for the linear, quadratic, and cubic polarizabilities, and $\hat{\varepsilon}$ is the dielectric constant. In the general case, the relationship of the response $\mathbf{P}(\mathbf{r}, t)$ to the field $\mathbf{E}(\mathbf{r}', t')$ is integral in nature.[171,172] This is due to the nonlocal nature of the interaction, and it leads to frequency and spatial dispersion. For example, for $\mathbf{P}^{(1)}$,

$$\mathbf{P}^{(1)}(r, t) = \int dr' \int_{-\infty}^{t} dt' \hat{\alpha}(r, r'; t, t')\mathbf{E}(r', t'). \tag{6.2}$$

In a crystalline stationary medium, $\hat{\varepsilon}(\mathbf{r}, \mathbf{r}'; t, t') + \hat{\varepsilon}(\mathbf{r}+\mathbf{b}, \mathbf{r}'+\mathbf{b}; t-t') = \sum_{\mathbf{Q}} \hat{\varepsilon}^{(\mathbf{Q})}(\mathbf{r}-\mathbf{r}', t-t')\exp(-i\mathbf{Q}\cdot\mathbf{r}')$, where $\mathbf{b}$ and $\mathbf{Q}$ are direct and reciprocal-lattice vectors,[172] so that we have the following expression for the Fourier components of the induction

$$\mathbf{D}(\mathbf{k}, \omega) = \sum_{\mathbf{Q}} \hat{\varepsilon}^{(\mathbf{Q})}(\mathbf{k}, \omega)\mathbf{E}(\mathbf{k}+\mathbf{Q}, \omega),$$
$$\hat{\varepsilon}^{(\mathbf{Q})}(\mathbf{k}, \omega) = \int d\rho \int_0^{\infty} d\tau\, \hat{\varepsilon}^{(\mathbf{Q})}(\rho, \tau)\exp[-i(\mathbf{k}\cdot\rho - \omega\tau)]. \tag{6.3}$$

Relationships analogous to Eqs. (6.2)–(6.3) hold[171] also for the polarizabilities $\hat{\beta}$ and $\hat{\gamma}$. The nonlinear Maxwell equation gives rise to the system

$$[n_{\mathbf{k}}^2\hat{\pi}_{\mathbf{k}} - \hat{\varepsilon}^{(0)}(\mathbf{k}, \omega)]\mathbf{E}(\mathbf{k}, \omega) - \sum_{\mathbf{Q}\neq 0} \hat{\varepsilon}^{(\mathbf{Q})}(\mathbf{k}, \omega)\mathbf{E}(\mathbf{k}+\mathbf{Q}, \omega) = 4\pi\mathbf{P}^{NL}(\mathbf{k}, \omega), \tag{6.4}$$

Here $n_{\mathbf{k}} = ck/\omega$, and $\hat{\pi}_{\mathbf{k}}$ is the operator for projection on a plane perpendicular to $\mathbf{k}$. As we know the fields $\mathbf{E}(\mathbf{k}, \omega)$ and $\mathbf{E}(\mathbf{k}+\mathbf{Q}, \omega)$, do not satisfy the Bragg condition $|\mathbf{k}| \approx |\mathbf{k}+\mathbf{Q}|$, and they are practically not coupled with one another. Thus we can omit the corresponding equations in the system (6.4).

Let a plane monochromatic pump wave $\mathbf{e}_1 E_1 \exp(i\mathbf{k}_1\cdot\mathbf{r} - i\omega_1 t)$ (+ complex conjugate) propagate in the medium in a direction far enough from the Bragg directions (single-wave approximation). If the single-wave approximation also holds for the supplementary wave of frequency $\omega_3 = \omega_1 - \omega_2$, then from (6.1) and (6.4), the nonlinear response $\mathbf{P}^{NL}$ at the signal frequency has the folfowing form:

$$\mathbf{P}^{NL}(\mathbf{k}_2, \omega_2) = \sum_{\mathbf{Q}} \Delta\hat{\alpha}^{(\mathbf{Q})}(\mathbf{k}_2, \omega_2)\mathbf{E}(\mathbf{k}_2+\mathbf{Q}, \omega_2), \tag{6.5}$$

Here $\Delta\hat{\alpha}^{(\mathbf{Q})}$ is the nonlinear increment to the linear polarizability $\alpha^{(\mathbf{Q})}(\mathbf{k}_2, \omega_2)$:

$$\Delta\hat{\alpha}^{(\mathbf{Q})} = [\hat{\gamma}^{(\mathbf{Q})}(\omega_2)\mathbf{e}_1\mathbf{e}_1 + \hat{\beta}^{(\mathbf{Q}_1)}(\omega_2)\mathbf{e}_1\hat{G}_3^*\hat{\beta}^{(\mathbf{Q}_1-\mathbf{Q})*}(\omega_2)\mathbf{e}_1]|E_1|^2, \tag{6.6}$$
$$\hat{G}_3 = 4\pi[n_3^2\hat{\pi}_{\mathbf{k}_3} - \hat{\varepsilon}^{(0)}(\mathbf{k}_3, \omega_3)]^{-1}; \tag{6.7}$$

Here $\hat{G}_3$ is the spectral Green's function in the single-wave approximation for the field of frequency ω_3, and $n_3 = c|\mathbf{k}_1+\mathbf{Q}_1-\mathbf{k}_2|/\omega_3$. The relationships (6.5)–(6.8) are a generalization of the results of Ref. 173, which were obtained in the single-wave approximation ($\mathbf{Q} = \mathbf{Q}_1 = 0$). The increment $\Delta\hat{\alpha}$ is proportional to the pump intensity, and it determines the dynamic and the statistical properties of the medium.

We are interested in the field of the signal $\mathbf{E}(\mathbf{r}, \omega_1)$ in the zone far from the scattering volume V. Upon writing the solution (6.4) in the form

$$\mathbf{E}(\mathbf{k}_2, \omega_2) = \sum_{\mathbf{Q}} \hat{G}^{(\mathbf{Q})}(\mathbf{k}_2, \omega_2)\mathbf{P}^{NL}(\mathbf{k}_2+\mathbf{Q}, \omega_2),$$

where $\hat{G}^{(\mathbf{Q})}(\mathbf{k}_2, \omega_2)$ is the $\mathbf{Q}$ component of the multiwave spectral Green's function of the system (6.4), we have the following expressions for $\mathbf{E}(\mathbf{r}, \omega_2) \equiv \mathbf{E}_2$:

$$\mathbf{E}_2 = \int d\mathbf{r}' \sum_{\mathbf{Q}} \hat{G}^{(\mathbf{Q})}(\mathbf{r}-\mathbf{r}', \omega_2)\exp(-i\mathbf{Q}\mathbf{r}')\mathbf{P}^{NL}(\mathbf{r}', \omega_2), \tag{6.8}$$
$$\hat{G}^{(\mathbf{Q})}(\rho, \omega_2) = (2\pi)^{-3}\int d\mathbf{k}\hat{G}^{(\mathbf{Q})}(\mathbf{k}, \omega_2)\exp(i\mathbf{k}\rho). \tag{6.9}$$

According to (6.8), the spectral intensity $P_{\omega\vartheta} = (cr^2/2\pi)\langle\mathbf{E}_2^*\cdot\mathbf{E}_2\rangle$ of the light, i.e., the power scattered per

unit intervals of frequency and angle, is proportional to the correlator $\langle P_i^{NL*}(\mathbf{r}, \omega_2) P_j^{NL}(\mathbf{r}', \omega_2')\rangle$, and it is defined in terms of the increment $\Delta\hat{\alpha}$. One can show this most simply by using the relation between the fluctuations in the presence of the pump and the cubic nonlinearity.[175] If, following Ref. 175, we convert to distributed quantities, then this relation acquires a form analogous to the linear fluctuation-dissipation theorem:

$$\langle P_i^{NL*}(\mathbf{r}, \omega_2) P_j^{NL}(\mathbf{r}', \omega_2')\rangle = i\hbar(2\pi)^{-4}[\Delta\alpha_{ji}(\mathbf{r}, \mathbf{r}'; \omega_2) - \Delta\alpha_{ji}^*(\mathbf{r}', \mathbf{r}; \omega_2)]\,\delta(\omega_2 - \omega_2'), \tag{6.10}$$

Here we assume that $\hbar\omega_3 \gg k_B T$. Now it remains only to find the coordinate Green's function (6.9).

For simplicity, let us restrict the treatment to the two-wave approximation. That is, we shall discuss the case in which only two reciprocal-lattice nodes ($Q=0$ and H) lie near the Ewald sphere for a signal of radius $|\varkappa_2| = \omega_2/c$, which depends on the angle ϑ. Let $\mathbf{s}_2$ be a unit vector in the direction of observation, and $\mathbf{n}_0$ be the normal to the surface in the crystal in the outward direction. As usual,[31,176] with account taken of the boundary conditions, we shall write $\mathbf{k}_2 = \varkappa_2(\mathbf{s}_2 + g\mathbf{n}_0)$, $g \ll 1$. We can neglect stimulated-scattering processes at low pump intensity, i.e., $\Delta\hat{\alpha}^{(\mathbf{Q})} \ll \hat{\alpha}^{(\mathbf{Q})}$. We can provisionally take the wave $\mathbf{k}_2$ to be the primary wave, and $\mathbf{k}_{2h} = \mathbf{k}_2 + \mathbf{H}$ to be the diffracted wave, although they are actually equivalent, and both are "generated" within the crystal in the presence of the pump. Then we get from (6.4) and (6.9) after integrating over g:

$$\hat{G}^{(\mathbf{Q})}(\mathbf{r}, \omega_2) = \frac{\omega_2^4}{\gamma_1 c^2}\sum_{m=1}^{2}\sum_{\mu=1}^{2}\hat{L}^{(\mathbf{Q})}(m, \mu)\exp(i\tilde{k}_\mu^{(m)} r), \tag{6.11}$$

$$\hat{L}^{(0)} = \frac{\pm p_m + \sqrt{p_m^2+1}}{2\sqrt{p_m^2+1}}\mathbf{e}_2^{(m)}\mathbf{e}_2^{(m)},$$

$$\hat{L}^{(\mathbf{H})} = \frac{\pm\exp(i\vartheta_h)}{2\sqrt{p_m^2+1}}\sqrt{\frac{\gamma_0}{\gamma_h}}\,\mathbf{e}_2^{(m)}\mathbf{e}_{2h}^{(m)}. \tag{6.12}$$

Here the polarization unit vectors $\mathbf{e}_2^{(m)}$ and $\mathbf{e}_{2h}^{(m)}$ for $m=1$ are perpendicular to the plane formed by the vectors $\mathbf{k}_2$ and $\mathbf{k}_{2h}$; for $m=2$, they lie in this plane; γ_0 and γ_h are the cosines of the angles between $\mathbf{n}_0$ and $\mathbf{s}_2$ and $\varkappa_2 + \mathbf{H}$, respectively. The upper and lower signs in (6.12) refer to the excitation points $\mu=1$ and 2. We assume that $\gamma_h > 0$ (the Laue case), i.e., the vectors $\mathbf{k}_2$ and $\mathbf{k}_{2h}$ are directed outward. The coefficients L determine the dynamic coupling between the spatially-conjugate modes $\mathbf{k}_2$ and $\mathbf{k}_{2h}$.

The parameter $p_m = -(2\Delta\omega\sin^2\vartheta_B/\omega_2|\varepsilon_m|)\sqrt{\gamma_0/\gamma_h}$ characterizes the degree of deviation of the signal frequency $\omega_2 = \omega_B + \Delta\omega$ from the so-called Bragg frequency $\omega_B(\mathbf{s}_2)$ as determined at the given angle $(\pi/2)+u$ between $\mathbf{s}_2$ and $\mathbf{H}$ by the relationship $\omega_B = cH/2\sin u$.[17] We also have the coefficient $\varepsilon_m = |\varepsilon_m|\exp(i\vartheta_h)$, $\varepsilon_m = \varepsilon^{(\mathbf{H})}(\mathbf{k}_2, \omega_2)C_m$, $\varepsilon^{(\mathbf{H})} = -(4\pi N_0 e^2/m\omega_2^2)F(\mathbf{H}) \sim 10^{-5}-10^{-6}$, $C_1 = 1$, $C_2 = \cos 2\vartheta_B$, and $\sin\vartheta_B = cH/2\omega_2$. The dispersion law $\tilde{\mathbf{k}}_\mu^{(m)}$ of the medium is determined by the contributions of the poles of the spectral Green's function in (6.9), and it is well known in the dynamical theory.[31,176]

Thus, from (6.8), (6.10), and (6.11), the spectral intensity of the inelastic scattering with account taken of the dynamical interaction of the signal waves is

$$P_{\omega\vartheta} = S_{\omega_2}\sum_{m\mu}\left[-\frac{4\pi\omega_2}{c}\sum_{\mathbf{QQ}'}L_{ij}^{(\mathbf{Q})*}L_{il}^{(\mathbf{Q}')}\Delta\tilde{\alpha}_{lj}^{(\mathbf{Q}-\mathbf{Q}')}\right]V_{\mu m}^{(e)},$$
$$\Delta\tilde{\alpha}_{lj}^{(\mathbf{Q}-\mathbf{Q}')} \equiv \frac{1}{2i}[\Delta\alpha_{lj}^{(\mathbf{Q}-\mathbf{Q}')}(\tilde{\mathbf{k}}_\mu^{(m)}+\mathbf{Q}', \omega_2) - \Delta\alpha_{lj}^{(\mathbf{Q}-\mathbf{Q}')}(\tilde{\mathbf{k}}_\mu^{(m)}+\mathbf{Q}', -\omega_2)], \tag{6.13}$$

Here $S_{\omega_2} = \hbar\omega_2^3/8\pi^3c^2$ is the spectral intensity of the vacuum fluctuations. The expression in square brackets in (6.13) can be treated as the nonlinear amplification coefficient of the $m\mu$-wave. For a crystalline plate of thickness l, the effective volume is

$$V_{\mu m}^{(e)} = \frac{A}{\gamma_1}\int_0^l \exp\left(-\frac{\mu_1 z}{\gamma_1} - \gamma_0\sigma_{\mu m}r_2\right)dz, \tag{6.14}$$

Here A, μ_1, and γ_1 are the cross section, absorption coefficient, and the cosine of the angle of incidence of the pumping; r_2 is the path length of the signal in the crystal from the point z to the exit face; $\sigma_{\mu m}$ is the dynamical absorption coefficient[31,176] of the signal, which is of resonance type in the Laue case with respect to the mismatch p_m, and which strongly differs for the excitation points $\mu = 1$ and 2 (the Borrmann effect for the scattered wave).

As Eqs. (6.13) and (6.12) imply, we can neglect dynamical effects in inelastic scattering at large frequency mismatches $|p_m| \gg 1$, since $L^{(\mathbf{H})} \approx 0$, and $L^{(0)} \approx 1$, so that in the single-wave approximation

$$P_{\omega\vartheta} = -S_{\omega_2}V^{(e)}\frac{4\pi\omega_2}{c}\mathbf{e}_2\Delta\hat{\alpha}^{(0)*}\mathbf{e}_2, \tag{6.15}$$

Here $\Delta\hat{\alpha}^{(0)''} < 0$ is the imaginary component of the increment $\Delta\alpha^{(0)}$; while the effective volume is determined by the ordinary linear absorption at the signal frequency, since $\sigma_{\mu m}(|p_m| \gg 1) = \mu_2/\gamma_0$. The relationship (6.15) permits us to relate simply the imaginary component $\Delta\alpha^{(0)}$ to the ordinary single-wave inelastic-scattering cross section $\sigma^{(0)}$:

$$\mathbf{e}_2\Delta\hat{\alpha}^{(0)*}\mathbf{e}_2 = \sigma^{(0)}(\omega, \vartheta)\frac{cn_0S_1}{4\pi\omega_2 S_{\omega_2}}, \tag{6.16}$$

Here n_0 is the density of scattering centers, and $S_1 = c|E_1|^2/2\pi$ is the pumping intensity.

One can also obtain the result (6.15) from the following simple physical arguments: the signal wave in the presence of the pump propagates according to the law $E_2 = E_{20}\exp[i(\omega_2/c)(n_2 z/\cos\vartheta) - i\omega_2 t]$, where the refractive index $n_2 = [1 + 4\pi\alpha_2^{(0)} + 4\pi\Delta\alpha_2^{(0)}]^{1/2}$. If we neglect the linear absorption, then in the case of a weak pump, the intensity of the signal wave $I_2 = I_{20}\exp(-4\pi\omega_2\Delta\alpha_2^{(0)''}z/c\cos\vartheta)$. Under the conditions of our problem, the role of the primer intensity I_{20} is played by the intensity of the zero-point fluctuations of the vacuum $\hbar\omega_2 d^3k_2/(2\pi)^3$, and the spectral scattering power is

[17] In the ordinary dynamical theory, in which the frequency of the waves is assumed to be fixed, the deviation parameter is the angular mismatch with the Bragg direction. Yet in inelastic-scattering experiments, the observation angle is fixed. Hence we have been treating a variant of the dynamical theory with frequency mismatch.

$$P_{\omega\vartheta} = S_{\omega_2} A \cos\vartheta\,(e^{gl/\cos\vartheta} - 1), \qquad (6.17)$$

Here $g = -(4\pi\omega_2/c)\Delta\alpha_2^{(0)\prime\prime}$ is the nonlinear amplification coefficient. The minus one in the parentheses corresponds simply to the fact that the intensity of the zero-point oscillations at the exit point of the crystal, which play the role of the background reference point, must be subtracted owing to their unobservability. For small amplification ($gl \ll 1$), Eq. (6.17) is reduced to (6.15).

A calculation of the nonlinear x-ray polarizabilities, which can be done, e.g., by using the results of Pine,[177] shows that the first term in (6.6) describes the Compton effect and Raman scattering, while the second term corresponds to plasmon and parametric scattering.[18] Actually, for an electron gas, e.g., in the long-wavelength approximation, the convolution $\mathbf{e}_2\hat{\beta}^{(0)}\mathbf{e}_1\cdot\mathbf{e}_3 = i\hat{\beta}_0 n_0 (c/\omega_3)(\mathbf{e}_1\cdot\mathbf{e}_2)(\mathbf{k}_3\cdot\mathbf{e}_3)$ differs from zero only for a longitudinal wave $\mathbf{k}_3$. After substitution into (6.6) and (6.16) with account taken of the equality $\hat{\pi}_{\mathbf{k}_3}\cdot\mathbf{e}_3 = 0$, this leads to the cross-section of (3.3) for scattering by plasmons.[173] One can derive this result also by a hydrodynamic treatment[179] or from the equation for the perturbed electron-distribution function.[180]

We have the following expression for the convolution of the cubic polarizability[173]:

$$\mathbf{e}_2\hat{\gamma}^{(0)}\mathbf{e}_1\mathbf{e}_1\mathbf{e}_2 = -\frac{e^4(\mathbf{e}_1\mathbf{e}_2)^2}{m^2\omega_1^2\omega_2^2\hbar V}\sum_{p_1}(f_{p_1+\hbar\mathbf{k}} - f_{p_1})[\omega(\mathbf{k}) - \omega - i\delta]^{-1},$$

Here f_p is the Fermi–Dirac distribution, and $\omega(\mathbf{k})$ is the spectrum of the single-particle excitations of (2.2). According to (6.6) and (6.16), this yields the inverted parabola of (2.8) for the Compton profile in the Hartree–Fock approximation for $k \geq 2k_F$, and a parabola with a rectilinear break for $k < 2k_F$, and also Eq. (3.1) in the random-phase approximation.[173]

One can show in exactly the same way that the quadratic polarizability for strongly bound electrons is determined by the relationships (5.3)–(5.5). This leads to the parametric-scattering power given by (5.6) with the synchronization law (5.2), while the cubic polarizability for $\omega_1 \gg \Omega_i$ and $|\mathbf{k}_1 - \mathbf{k}_2|\, a < 1$ corresponds to the Raman x-ray scattering cross section of (4.4).

Thus the phenomenological description and the micro-approach are equivalent when taken within the framework of identical approximations.

Interestingly, the extinction coefficient $\sigma^{(0)}(\vartheta)n_0$ of parametric and Raman scattering in optics is of the order of 10^{-7} cm^{-1}, whereas in the x-ray range these quantities are of the order of 10^{-9} and 10^{-2} cm^{-1} for parametric and Compton scattering, respectively. We can easily note that such significant values of the cross sections for x-ray inelastic scattering are explained by the large value of the spectral intensity of the vacuum fluctuations S_{ω_2} in (6.15), which is 12 orders of magnitude larger than in the optical range, and which compensates the smallness of the nonlinear x-ray polarizabilities ($S_{\omega_2} \sim 10$ W/cm^2 sr·Hz at $\lambda_2 \sim 1$ Å). Hence such classical nonlinear effects as harmonic generation and mixing, etc., will apparently not have such a real significance in the x-ray range as in the nonlinear optics of the visible and infrared ranges. Yet the smallness of the nonlinear polarizabilities and the large width of the inelastic-scattering spectral line leads[173] to extremely large values of the pump intensity ($\sim 10^{18}$ W/cm^2) that it takes to attain, e.g., an amplification coefficient of the order of 1 cm^{-1}.

7. COHERENT EFFECTS IN INELASTIC SCATTERING

In inelastic x-ray scattering in perfect enough single crystals, one can easily distinguish certain scattering directions in which the Bragg conditions will be satisfied for the signal waves in the medium. Owing to dynamical exchange between the modes $\mathbf{k}_2$ and $\mathbf{k}_{2h} = \mathbf{k}_2 + \mathbf{H}$, energy redistribution must occur here, and emission at the frequency ω_2 can be observed in new directions that had previously been forbidden by the laws of conservation of energy and momentum. Now the lattice will take up part of the momentum $\mathbf{H}$. Thus this amounts to interference of the inelastically scattered waves, which is a consequence of spatial (lattice) coherence. The directions in which coherent effects in inelastic scattering should be manifested are determined by the intersection lines of the surface $k_2(\mathbf{s}_2)$ that is formed by the ends of the vectors $\mathbf{k}_2$ having their origin at the midpoint of the vector $\mathbf{H}$ with planes perpendicular to $\mathbf{H}$ and contacting its ends. This is equivalent to the condition $\omega_{20}(\mathbf{s}_2) = \omega_B(\mathbf{s}_2)$ that the inelastic-scattering frequency at the center of the line is equal to the Bragg frequency.

According to (6.12) and (6.13), coherent effects in inelastic scattering begin to be manifested when the mismatch p_m approaches zero. In a small neighborhood of ω_B, the coefficients L of (6.12) differ from zero or unity. This leads to a considerable difference of the inelastic-scattering spectral line from the single-wave value of (6.15). Let us briefly examine the manifestation of coherent effects with the example of Compton scattering. If we keep in (6.13) the terms that give the major contribution, we have the following expression for the differential cross-section in the two-wave approximation:

$$\sigma(\omega, \vartheta) = \sum_{\mu m}\frac{V_{\mu m}^{(e)}}{V}\left[D_{\mu m}^{(00)}(\mathbf{e}_2^{(m)}\mathbf{e}_1)^2\sigma^{(0)}(\omega, \vartheta) + D_{\mu m}^{(\mathbf{HH})}(\mathbf{e}_{2h}^{(m)}\mathbf{e}_1)^2\sigma^{(0)}(\omega, \vartheta_h)\right]\left[\sum_m (\mathbf{e}_2^{(m)}\mathbf{e}_1)^2\right]^{-1}, \qquad (7.1)$$

Here ϑ_h is the angle between $\mathbf{k}_{2h}$ and $\mathbf{k}_1$, and $D_{\mu m}^{(\mathbf{QQ}')} = L^{(\mathbf{Q})*}L^{(\mathbf{Q}')}$. If we can neglect absorption, i.e., $V_{\mu m}^{(e)} = V$, then the summation over μ in (7.1) pertains only to the dynamical coefficients $D_{\mu m}$. According to (6.12),

$$\sum_\mu D_{\mu m}^{(00)} = 1 - \frac{\pi\Delta\omega_B}{2}g(\Delta\omega), \qquad (7.2a)$$

[18] In optics, the term γ describes scattering by infrared-inactive lattice vibrations, while the second term describes scattering by polaritons and longitudinal lattice vibrations. An expression analogous to (6.6) but with the rank of the tensor $\hat{\beta}$ increased by unity and that of $\hat{\gamma}$ by two describes quadratic inelastic scattering (scattering of light by light and three-photon Raman scattering).[178]

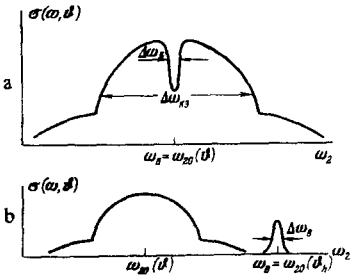

FIG. 16. Cross-section for the coherent Compton effect in the two-wave approximation. a) Spectral cross-section for scattering in the direction $\mathbf{s}_2$ at which $\omega_B(\mathbf{s}_2) = \omega_{20}(\vartheta)$; the depth of the gap amounts to $0.5\sigma^{(0)}(\omega_1 - \omega_B, \vartheta)$; b) scattering profile in the case $\omega_B(\mathbf{s}_2) = \omega_{20}(\vartheta_h)$; amplitude of the peak is $0.5\sigma^{(0)}(\omega_1 - \omega_B, \vartheta_h)\gamma_0/\gamma_h$ (for the sake of argument $\omega_B > \omega_{20}(\vartheta) + 0.5\Delta\omega_{CE}$).

$$\sum_{\mu} D_{\mu m}^{(\mathbf{HH})} = \frac{\pi\Delta\omega_B}{2} g(\Delta\omega)\frac{\gamma_0}{\gamma_h}, \qquad (7.2b)$$

where $\Delta\omega_B = (\pi\omega_2 |\varepsilon_m|/2\sin^2\vartheta_B)\sqrt{\gamma_h/\gamma_0}$ is the effective width normalized to the unit of the Lorentz line $g(\omega_2 - \omega_B)$, $g(0) = 1/\pi\Delta\omega_B$).

If the direction of observation $\mathbf{s}_2$ is such that the frequency ω_B lies within the Compton line $\sigma^{(0)}(\omega, \vartheta)$, then, as we see from (7.2a), the first term in (7.1) amounts to a spectral distribution that consists of the ordinary Compton profile with a narrow (since $\Delta\omega_B \ll \Delta\omega_{CE}$) gap at a frequency ω_B of Lorentzian form (Fig. 16a). The amplitude of the gap amounts to exactly half of the intensity $\sigma^{(0)}(\omega_1 - \omega_B, \vartheta)$. The second term in (7.1) has a simple physical meaning: it describes the process of pumping of energy from the mode $\mathbf{k}_{2h}$ that is scattered at the angle ϑ_h to the mode $\mathbf{k}_2$ in the direction of observation, so that if ω_B falls in the spectral interval of $\sigma^{(0)}(\omega, \vartheta_h)$, then a Lorentzian peak must be fixed in the direction $\mathbf{s}_2$. Ordinary inelastic scattering occurs in this same direction with the cross-section $\sigma^{(0)}(\omega, \vartheta)$ (Fig. 16b). In Ref. 181 this phenomenon has been called the coherent Compton effect (CCE).[19]

As Eq. (7.1) implies, one should observe CCE lines in the frequency-integrated distribution $\sigma(\vartheta)$ on the background of the almost uniform incoherent Compton effect. The lines have a fine angular structure[20] that depends on whether an excess or deficiency of radiation occurs in this direction. If the vectors $\mathbf{k}_1$ and $\mathbf{H}$ are not perpendicular, then the angular spectrum amounts to pairs of close-lying lines, one of which is brighter than the background, while the other is darker. Since the narrow gap scans along the Compton profile as the angle ϑ is varied, the angular line copies the shape of the frequency distribution. In order to estimate the contrast R (i.e., the ratio of the excess (or deficiency) of intensity at the center of the line to the Compton background) in the case of well-resolved lines, one can use the relationship $R = R_0 = (\pi/2)(\Delta\omega_B/\Delta\omega_{CE})$. When $\mathbf{k}_1 \perp \mathbf{H}$, the lines coincide, and the contrast is $R_0[1 - (\gamma_0/\gamma_h)]$. If $\gamma_0 = \gamma_h$, then the lines vanish, which is a manifestation of the complete symmetry in this experimental geometry.

TABLE I. Width of the Bragg gap, contrast, and line displacement in the coherent Compton effect.

Crystal	Silicon				Germanium			
Radiation	Cu K_α		Mo K_α		Cu K_α		Mo K_α	
Reflection	111	220	111	220	111	220	111	220
$\Delta\omega_B$, eV	3.2	1.4	6.9	3.1	9.1	4.0	19.7	8.7
R_0, %	9	3.9	19	8.7	25	11	55	24
$\Delta\psi$, minutes of angle	28	46	27	45	27	44	25	41

In a thick crystal, i.e., with $y = \mu_1 l \gg 1$, the equivalence of the excitation points breaks down, even in the case where $\gamma_0 = \gamma_h$. Owing to anomalous transmission, the volume $V_{\mu m}^{(e)}$ for scattering into the CCE line can exceed considerably the "background" volume, and the contrast should increase: $R = R_0 W(y)$. Thus, if $\sigma_{\mu m}^{\min} = 0.05\mu_1$, and $y = 1, 2, 3, 4$, and 5, then the coefficient W is equal respectively to 0.54, 2, 5.2, 11.5, and 25.2. Since the polarizability ε_m is proportional to the structure factor $F(\mathbf{H})$ inclusive of the Debye–Waller factor, the width $\Delta\omega_B$ of the gap and the contrast of the CCE line should depend on the temperature.

One must have rather perfect single crystals to observe the coherent Compton effect, preferably with a thickness sufficient to suppress the incoherent Compton effect. Certain estimates of a proposed experiment are given in Ref. 181. Table I gives values of the width $\Delta\omega_B$, the contrast R_0 ($\Delta\omega_{CE} \approx 56$ eV when $k \approx 2k_F$), and the change $\Delta\psi$ in the polar angle[21] of the CCE line with increase in the azimuthal angle from 0 to 180° for $\mathbf{k}_1 \perp \mathbf{H}$ in the case of the (111) and (220) reflections of Compton quanta in silicon and germanium.[184]

Analogous arguments hold also when one treats coherent effects in plasmon and Raman scattering, except that one must replace $\sigma_{CE}^{(0)}$ by $\sigma_{PS}^{(0)}$ or $\sigma_{RS}^{(0)}$. In the case of parametric scattering, $\Delta\omega_B \gg \Delta\omega_{PS}$, and an account for Bragg interaction leads to "repulsion" of the synchronization ellipsoids of (5.2) that correspond to the nodes Q and Q' ($\mathbf{Q} - \mathbf{Q}' = \mathbf{H}$) in the vicinity of their intersection lines. The frequency splitting should be of the order of $\Delta\omega_B$, and the angular splitting should be $\sim |\varepsilon_m| \sim 10^{-5}$–$10^{-6}$ radians.

The slightly bent interference Compton lines that have been observed in a number of studies[185] in scattering in mosaic crystals can be explained[186] by using systems of equations of the Zachariasen[187] type for the intensities of the "primary" and "diffracted" waves, but with zero boundary conditions and with distributed noise

[19] A dynamical treatment of the angular, (i.e., integrated over the frequency) thermal-diffuse-scattering spectrum in thick crystals had been given earlier by Afanas'ev *et al.*[182] within the framework of the microapproach.

[20] On the whole they recall the Kikuchi lines in electron diffraction[183] in shape and mechanism of production.

[21] The displacement $\Delta\psi$ characterizes the degree of deviation of the "primary" and the "diffracted" Compton lines from parallelism, which is due to the dependence of the Compton frequency on the scattering angle (see Ref. 181 for more details).

TABLE II. Some characteristics of different types of inelastic scattering.

Scattering	Angle ϑ, degrees	Cross-section	Energy $\hbar\omega$, eV	$\Delta\omega_{IS}$, eV	Quanta/sec·10⁻³ sr	
					DESY	FIAN
Compton	180	1	605	244	$7.7\cdot10^5$	$1.5\cdot10^6$
Plasma	10	$2.2\cdot10^{-1}$	22	10	$8.5\cdot10^4$	$1.7\cdot10^5$
Raman	30	$6.6\cdot10^{-2}$	112	29	$2.5\cdot10^4$	$5\cdot10^4$
Parametric	40	$1.1\cdot10^{-7}$	$6.2\cdot10^3$	0.03	$8.6\cdot10^{-2}$	0.17

sources added to the right-hand sides with an intensity proportional to $\sigma_{CE}^{(0)}(\omega, \vartheta) S_1$.

Thus inelastic scattering of x rays is an important method of studying the electronic structure of matter. Further progress along this line is being hindered by the lack of powerful x-ray sources. We should note that the use of synchrotron x rays, which is characterized by high spectral intensity, small divergence, high degree of polarization, and by the possibility of regulating the frequency and emission spectrum over a broad range, permits us to hope to get new interesting results.

For comparison of the effectiveness of different types of x-ray inelastic scattering, Table II gives the scattering cross sections in beryllium in terms of their ratio to σ_T, the energies $\hbar\omega$ of the shifts, and the widths of the lines. The last two columns give the numbers of quanta scattered per second in a solid angle of 10^{-3} sr. The pump intensities at a wavelength of 1 Å amount to 7.8×10^{10} and 3.7×10^{10} quanta/sec·cm² in an interval of 1 eV. These values correspond to the characteristics of the DESY (7.5 GeV) and FIAN (1.3 GeV with special magnets) synchrotrons.[188] The thickness of the specimens is 1 cm, and the cross section is 0.27×1 cm or 1.14×1 cm, respectively, as determined by the slit width and the divergence of the synchrotron radiation.

Study of inelastic scattering is currently being conducted exclusively in the optical (~$3-10\times10^3$ Å) and x-ray (~0.1–2 Å) ranges. It is of no lesser interest to study inelastic scattering in the far ultraviolet and soft x-ray regions (~10–1000 Å), in which synchrotron radiation is perhaps the only effective source. As an example of an application, we can cite the possible observation of Raman scattering by excitonic polaritons, which have an energy of several electron volts.[22)]

In conclusion, the authors express their deep gratitude to D. N. Klyshko for aid and useful discussions of the problems of the phenomenological theory of inelastic scattering.

[22)] The authors are grateful to V. M. Agranovich and V. V. Mikhaĭlin, who called their attention to this fact.

[1] J. W. M. Du Mond, Rev. Mod. Phys. **5**, 1 (1933).
[2] M. Cooper, Adv. Phys. **20**, 453 (1971).
[3] J. A. Gray, J. Franklin Inst. 633 (1920).
[4] A. H. Compton, Bull. Nat. Res. Coun. Wash. **4** (20), 19 (1922); Phys. Rev. **21**, 207, 483 (1923).
[5] P. Debye, Phys. Zs. **24**, 161 (1923).
[6] P. A. Ross, Phys. Rev. **22**, 201, 524 (1923). H. M. Sharp, *ibid.* **26**, 691 (1925). F. L. Nutting, *ibid.* **26**, 1267 (1930).
[7] A. H. Compton, *ibid.* **22**, 409 (1923).
[8] G. E. M. Jauncey, *ibid.* **24**, 204 (1924); **25**, 314, 723 (1925).
[9] J. W. M. Du Mond, *ibid.* **33**, 643 (1929).
[10] J. W. M. Du Mond, *ibid.* **36**, 146 (1930); **39**, 166 (1932). J. W. M. Du Mond and H. A. Kirkpatrick, *ibid.* **37**, 136; **38**, 1094 (1931); **52**, 419 (1937). J. W. M. Du Mond, H. A. Kirkpatrick and L. Alden, *ibid.* **40**, 165 (1932). H. A. Kirkpatrick and J. W. M. Du Mond, *ibid.* **54**, 802 (1938).
[11] W. Heitler, The Quantum Theory of Radiation, 3rd Ed., Clarendon Press, Oxford, 1954 (Russ. Transl., IL, M., 1956).
[12] G. F. Chew, Phys. Rev. **80**, 196 (1950).
[13] P. M. Platzman and N. Tzoar, *ibid.* **A139**, 410 (1965).
[14] P. Eisenberger and P. M. Platzman, *ibid.* **A2**, 415 (1970).
[15] N. G. Alexandropoulos, S. H. Parks, and M. Kuriyama, Phys. Lett. **A35**, 369 (1971).
[16] W. E. Duncanson and C. A. Coulson, Proc. Phys. Soc. **57**, 190 (1945). **A65**, 825 (1952). C. A. Coulson and N. H. March, *ibid.* **63**, 367 (1950).
[17] N. H. March, *ibid.* **67**, 9 (1954). G. E. Kilby, *ibid.* **86**, 1037 (1965).
[18] R. J. Weiss, A. Harvey, and W. C. Phillips, Phil. Mag. **17**, 241 (1968).
[19] A. H. Compton, Phys. Rev. **23**, 763; *ibid.* **24**, 168 (1924).
[20] P. A. Ross and P. Kirkpatrick, *ibid.* **46**, 668 (1934).
[21] F. Bloch, *ibid.* 46, 674.
[22] R. Currat, P. D. De Cicco, and R. Kaplov, *ibid.* **B3**, 243 (1971).
[23] R. Currat, P. D. De Cicco, and R. J. Weiss, *ibid.* **B4**, 4256.
[24] G. Wentzel, Zs. Phys. 43, 1, 779 (1927); **58**, 348 (1929).
[25] F. Schnaidt, Ann. d. Phys. **21**, 89 (1934). M. Gavrila, Phys. Rev. **A6**, 1348, 1360 (1972). I. G. Kaplan and G. L. Yudin, Zh. Eksp. Teor. Fiz. 69, 9 (1975) [Sov. Phys. JETP **42**, 4 (1975)].
[26] P. Eisenberger, Phys. Rev. **A5**, 628 (1972).
[27] M. Cooper and J. A. Leak, Phil. Mag. **13**, 603 (1966); 15, 1201 (1967).
[28] N. G. Alexandropoulos and K. D. Alexopoulos, Phys. Rev. A140, 597 (1965).
[29] W. C. Phillips and R. J. Weiss, *ibid.* 171, 790 (1968).
[30] T. Fukamachi and S. Hosoya, J. Phys. Soc. Japan **28**, 161 (1970). R. J. Weiss, Phil. Mag. 28, 1161 (1973). T. Paakkari and P. Suortti, Phys. Rev. B9, 1756 (1974).
[31] R. W. James, The Crystalline State, Vol. 2. The Optical Principles of the Diffraction of X-Rays, George Bell & Sons, London, 1948 (Russ. Transl., IL, M., 1950).
[32] W. Schülke and U. Berg, Phys. Stat. Sol. 23, K87 (1967).
[33] M. Cooper, J. A. Leak, and R. J. Weiss, Phil. Mag. **12**, 797 (1965).
[34] V. P. Tsvetkov and L. V. Shevtsov, Fiz. Tverd. Tela (Leningrad) 15, 3074 (1973) [Sov. Phys. Solid State 15, 2047 (1974)].
[35] W. A. Rachinger, J. Sci. Instrum. **25**, 254 (1948).
[36] T. Fukamachi and S. Hosoya, J. Phys. Soc. Japan **29**, 736 (1970).
[37] D. Esslinger, R. Hosemann, A. Müller, and D. Weick, J. Appl. Phys. 45, 4100 (1974).
[38] P. Paatero, S. Manninen, and T. Paakkari, Phil. Mag. 30, 1281 (1974).
[39] P. Eisenberger and W. A. Reed, Phys. Rev. **B9**, 3237 (1974). R. Ribberfors, *ibid.* **B12**, 2067, 3136 (1975).
[40] J. W. M. Du Mond, *ibid.* **36**, 1685 (1930). W. C. Phillips and A. K. Chin, Phil. Mag. 27, 87 (1973). B. G. Williams, P. Pattison, and M. J. Cooper, *ibid.* **30**, 307 (1974). J. Felsteiner, P. Pattison, and M. Cooper, *ibid.* 30, 537. P. Pattison, S. Manninen, J. Felsteiner, and M. Cooper, *ibid.* 30, 973. V. Halonen, B. G. Williams, and T. Paakkari, Phys. Fennica 10, 107 (1975). A. C. Tanner and I. R. Epstein, Phys. Rev. A13, 335; A14, 313, 328 (1976).
[41] M. Cooper and B. G. Williams, Phil. Mag. 17, 1079 (1968).

R. J. Weiss, *ibid.* **25**, 1511; **26**, 761 (1972); Phys. Rev. Lett. **24**, 883 (1970). W. C. Phillips and R. J. Weiss, Phys. Rev. **B6**, 4213 (1972).
[42]R. J. Weiss, Phil. Mag. **14**, 403 (1966); **27**, 1461 (1973). W. C. Phillips, Phys. Rev. **B7**, 1047 (1973).
[43]J. Felsteiner, R. Fox, and S. Kahane, Phys. Lett. **A33**, 442 (1970). T. Fukamachi, S. Hosoya, K. Iway, and K. Hayakawa, *ibid.* **A42**, 477 (1973). S. Wakoh, T. Fukamachi, S. Hosoya, and J. Yamashita, J. Phys. Soc. Japan **38**, 1601 (1975).
[44]J. Felsteiner, R. Fox, and S. Kahane, Sol. State Comm. **9**, 61, 457 (1971); Phys. Rev. **B6**, 4689 (1972). T. Paakkari, S. Manninen, O. Inkinen, and E. Linkonen, *ibid.* **B6**, 351 (1972). T. Paakkari and S. Manninen, *ibid.* **B8**, 3765 (1973). S. Manninen, T. Paakkari, and K. Kajante, Phil. Mag. **29**, 167 (1974).
[45]T. Fukamachi, S. Hosoya, Y. Hosokawa, and H. Hirata, Phys. Stat. Sol. **a10**, 437 (1972).
[46]W. A. Reed and P. Eisenberger, Phys. Rev. **B6**, 4596 (1972); **B9**, 3242 (1974). K. -F. Berggren, F. Martino, P. Eisenberger, and W. A. Reed, *ibid.* **B13**, 2292 (1976).
[47]S. Berko and J. S. Plaskett, *ibid.* **112**, 1877 (1958). E. Daniel and S. H. Vosko, *ibid.* **120**, 2041 (1960). A. W. Overhauser, *ibid.* **B3**, 1888 (1971). J. Lam, *ibid.* 3243.
[48]B. I. Lundquist and C. Lyden, *ibid.* **B4**, 3360. P. Eisenberger, L. Lam, P. M. Platzman, and P. Schmidt, *ibid.* **B6**, 3671 (1972). C. S. Wang and J. Callaway, *ibid.* **B11**, 2417 (1975). S. Wakoh and J. Yamashita, J. Phys. Soc. Japan **35**, 1402, 1406 (1973). B. W. Tan, J. Phys. **F3**, 1716 (1973).
[49]G. E. Kilby, Proc. Phys. Soc. **82**, 900 (1963).
[50]W. A. Reed, P. Eisenberger, F. Martino, and K. -F. Bergren, Phys. Rev. Lett. **35**, 114 (1975). O. Aikala, Phil. Mag. **32**, 333 (1975); **33**, 603 (1976).
[51]K. -F. Bergren, Sol. State Comm. **9**, 861 (1971). K. -F. Bergren, and F. Martino, Phys. Rev. **B3**, 1509 (1971). O. Aikala and K. Mansikka, Phil. Mag. **28**, 997 (1973). O. Aikala, *ibid.* **31**, 935 (1975).
[52]O. Aikala, V. Jokela, and K. Mansikka, J. Phys. **C6**, 1116 (1973).
[53]R. J. Weiss, Phil. Mag. **24**, 1477 (1971).
[54]N. G. Alexandropoulos, Phys. Rev. **150**, 610 (1966). R. J. Weiss and W. C. Phillips, *ibid.* **176**, 900 (1968); **182**, 923 (1969). R. J. Weiss, Phil. Mag. **26**, 153 (1972); **32**, 245 (1975).
[55]R. J. Weiss, Acta Cryst. **A25**, 248 (1969).
[56]S. A. Vorob'ev, Prokhozhdenie beta-chastits cherez kristally (Passage of Beta Particles Through Crystals), Atomizdat, M., 1975.
[57]P. Nozières and D. Pines, Phys. Rev. **113**, 1254 (1959).
[58]Y. Ohmura and N. Matsudaira, J. Phys. Soc. Japan **19**, 1355 (1964).
[59]C. Zener, Phys. Rev. **48**, 573 (1935). P. Debye, Phys. Zs. **38**, 161 (1937).
[60]J. Lindhard, Kgl. Danske Videnskab. Selskab. Mat.-Fys. Medd. **28**, 8 (1954).
[61]A. Theodossiou and P. Vosnidis, Phys. Rev. **145**, 458 (1966).
[62]G. G. Cohen *et al.*, Sol. State Comm. **10**, 95 (1972).
[63]W. Schülke, U. Berg, and O. Brümmer, Phys. Stat. Sol. **35**, 227 (1969).
[64]D. Pines, Elementary Excitations in Solids, Benjamin, New York 1963 (Russ. Transl., Mir, M., 1965).
[65]P. M. Platzman and P. A. Wolff, Waves and Interactions in Solid State Plasmas, Academic Press, New York, 1973 (Russ. Transl., Mir, M., 1975).
[66]D. Pines and D. Bohm, Phys. Rev. **85**, 338 (1952).
[67]P. M. Platzman, *ibid.* **139**, A379 (1965). Y. C. Lee and N. Tzoar, *ibid.* **140**, 396 (1965). P. A. Wolff, *ibid.* **171**, 436 (1968).
[68]A. Mooradian and G. B. Wright, Phys. Rev. Lett. **16**, 999 (1966). A. Mooradian and A. L. McWhorter, *ibid.* **19**, 849 (1967). C. K. N. Patel and R. E. Slusher, *ibid.* **22**, 282 (1969).
[69]I. I. Sobel'man and E. L. Feinberg, Zh. Eksp. Teor. Fiz. **34**, 494 (1958) [Sov. Phys. JETP **7**, 339 (1958)].
[70]V. M. Agranovich and V. L. Ginzburg, Zh. Eksp. Teor. Fiz. **40**, 913 (1961) [Sov. Phys. JETP **13**, 638 (1961)].
[71]L. D. Landau, Zh. Eksp. Teor. Fiz. **16**, 574 (1946).
[72]G. Priftis *et al.*, Phys. Lett. **A27**, 577 (1968).
[73]G. Priftis, Phys. Rev. **B2**, 54 (1970).
[74]D. M. Miliotis, *ibid.* **B3**, 701 (1971).
[75]G. D. Priftis, *ibid.* **B8**, 3134 (1973).
[76]D. Marinos and D. Miliotis, Phys. Stat. Sol. **b68**, K133 (1975).
[77]C. Koumelis, D. Leventouri, and K. Alexopoulos, *ibid.* **46**, K89 (1971). Th. Kokkinakis and K. Alexopoulns, Phys. Rev. Lett. **28**, 1632 (1972). C. Koumelis and D. Leventouri, Phys. Rev. **B7**, 181 (1973).
[78]T. Suzuki and A. Tanokura, J. Phys. Soc. Japan **29**, 972 (1970).
[79]A. Tanokura, N. Hirota, and T. Suzuki, *ibid.* **27**, 515 (1969); **28**, 1382 (1970). T. Suzuki and A. Tanokura, *ibid.* **30**, 892 (1971).
[80]N. G. Alexandropoulos, *ibid.* **31**, 1790.
[81]P. Eisenberger, P. M. Platzman, and K. C. Pandy, Phys. Rev. Lett. **31**, 311 (1973).
[82]P. M. Platzman and P. Eisenberger, *ibid.* **33**, 152 (1974).
[83]P. Eisenberger, P. M. Platzman, and P. Schmidt, *ibid.* **34**, 18 (1975).
[84]P. Eisenberger and P. M. Platzman, Phys. Rev. **B13**, 934 (1976).
[85]W. Schülke and W. Lautner, Phys. Stat. Sol. **b66**, 211 (1974).
[86]Yu. A. Rozenberg, V. F. Karpenko, and L. I. Kleshchinskiĭ, Fiz. Tverd. Tela (Leningrad) **18**, 1841 (1976) [Sov. Phys. Solid State **18**, 1073 (1976)].
[87]K. D. Alexopoulos, Zs. Naturforsch. **28a**, 550 (1973).
[88]K. L. Kliewer and H. Raether, Phys. Rev. Lett. **30**, 971 (1973); J. Phys. **C7**, 689 (1974).
[89]N. Matsudaira and S. Nagai, J. Phys. Soc. Japan **36**, 234 (1974).
[90]A. Pimpale and C. Mande, J. Phys. **C4**, 2593 (1971); **C8**, 2463 (1975).
[91]P. Zacharias, *ibid.* **C7**, L26 (1974).
[92]N. D. Mermin, Phys. Rev. **B1**, 2362 (1970).
[93]P. Vashishta and K. S. Singwi, *ibid.* **B6**, 875 (1972). K. N. Pathak and P. Vashishta, *ibid.* **B7**, 3649 (1973).
[94]P. M. Platzman and P. Eisenberger, Sol. State Comm. **14**, 1 (1974).
[95]R. K. Kalia and G. Mukhopadhyay, *ibid.* **15**, 1243 (1974).
[96]G. Mukhopadhyay, R. K. Kalia, and K. S. Singwi, Phys. Rev. Lett. **34**, 950 (1975).
[97]D. F. Dubois, Ann. Phys. **7**, 174; **8**, 24 (1959). V. V. Rumyantsev, Fiz. Tverd. Tela (Leningrad) **9**, 2377 (1967); **10**, 2275 (1968) [Sov. Phys. Solid State **9**, 1860 (1968); **10**, 1793 (1969)].
[98]M. Hasegawa, J. Phys. Soc. Japan **31**, 694 (1971). V. V. Rumyantsev, Fiz. Tverd. Tela (Leningrad) **13**, 2038 (1971) [Sov. Phys. Solid State **13**, 1709 (1972)].
[99]T. Aiyama and K. Yada, J. Phys. Soc. Japan **36**, 1554 (1974).
[100]K. C. Pandey, P. M. Platzman, P. Eisenberger, and E.-Ni Foo, Phys. Rev. **B9**, 5046 (1974).
[101]W. M. Saslow and G. F. Reiter, *ibid.* **B7**, 2995 (1973).
[102]S. L. Adler, *ibid.* **126**, 413 (1962). N. Wiser, *ibid.* **129**, 62 (1963).
[103]H. Ehrenreich and M. L. Cohen, *ibid.* **115**, 786 (1959).
[104]J. P. Walter and M. L. Cohen, *ibid.* **B5**, 3101 (1972).
[105]S. J. Sramek and M. L. Cohen, *ibid.* **B6**, 3800.
[106]M. S. Haque and K. L. Kliewer, *ibid.* **B7**, 2416 (1973).
[107]E.-Ni Foo and J. J. Hopfield, *ibid.* **173**, 635 (1968).

[108]a) Yu. E. Lozovik, V. N. Nishanov, and V. I. Yudson, in: Proc. of the 1st Soviet-American Symposium, v. 1, M., "Nauka", 1976, p. 237. b) J. C. Ashley, T. L. Ferrell and R. H. Ritchi, Phys. Rev. B10, 554 (1974).
[109]A. Smekal, Naturwissenschaften 11, 873 (1923).
[110]C. V. Raman, Indian J. Phys. 2, 387 (1928).
[111]K. S. Krishnan, Nature 122, 961 (1928).
[112]D. Mitchell and B. Davis, Phys. Rev. 31, 1119 (1928). B. Davis and D. P. Mitchell, *ibid.* 32, 331. D. Coster, I. Nitta, and W. J. Thijssen, Nature 124, 230 (1929).
[113]D. P. Mitchell, Phys. Rev. 33, 871 (1929).
[114]B. Davis and H. Purks, *ibid.* 34, 1.
[115]K. Das Gupta, Nature 166, 536 (1950); 167, 313 (1951); Phys. Rev. 128, 2181 (1962).
[116]K. Das Gupta, Phys. Rev. Lett. 3, 38 (1959).
[117]K. Das Gupta, *ibid.* 13, 338 (1964).
[118]T. Suzuki, J. Phys. Soc. Japan 21, 2087 (1966).
[119]A. Faessler and P. Mühle, Phys. Rev. Lett. 17, 4 (1966).
[120]W. Ehrenberg, Zs. Phys. 53, 234 (1929). W. Kast, *ibid.* 58, 519. D. Coster, Nature 123, 642 (1929). J. A. Bearden, Phys. Rev. 35, 1427; 36, 791 (1930). N. S. Gingrich, *ibid.* 35, 1444; 36, 1050. R. J. Weiss, *ibid.* 140, A1867 (1965).
[121]A. Sommerfeld, *ibid.* 50, 38 (1936).
[122]Y. Mizuno and Y. Ohmura, J. Phys. Soc. Japan 22, 445 (1967).
[123]T. Suzuki, *ibid.* p. 1139.
[124]T. Suzuki, T. Kishimoto, T. Kaji, and T. Suzuki, *ibid.* 29, 730 (1970).
[125]T. Suzuki and H. Nagasawa, *ibid.* 39, 1579 (1975).
[126]N. G. Alexandropoulos and G. G. Cohen, Phys. Rev. 187, 455 (1969).
[127]N. G. Alexandropoulos, *ibid.* B1, 4115 (1970); B3, 2670 (1971).
[128]G. G. Cohen, N. G. Alexandropoulos and M. Kuriyama, *ibid.* B8, 5427 (1973).
[129]N. G. Alexandropoulos, G. G. Cohen, and M. Kuriyama, Phys. Rev. Lett. 33, 699 (1974). N. G. Alexandropoulos and G. G. Cohen, *ibid.* 35, 1182 (1975).
[130]M. Kuriyama and N. G. Alexandropoulos, J. Phys. Soc. Japan 31, 561 (1971). M. Kuriyama, Acta Cryst. A27, 634 (1971).
[131]S. Doniach, P. M. Platzman and J. T. Yue, Phys. Rev. B4, 3345 (1971).
[132]P. Mühle, Phys. Lett. A44, 315 (1973).
[133]F. A. Babushkin, Izv. vuzov, ser. Fizika, No. 9, 26 (1971); F. A. Babushkin, Acta Phys. Polonica A40, 183 (1971).
[134]G. D. Priftis, Phys. Lett. A49, 281 (1974).
[135]M. G. Gavrilov and A. V. Davydov, Pis'ma Zh. Eksp. Teor. Fiz. 21, 569 (1975) [JETP Lett. 21, 267 (1975)].
[136]C. J. Sparks, Jr., Phys. Rev. Lett. 33, 262 (1974).
[137]T. Aberg and J. Utriainen, *ibid.* 22, 1346 (1969).
[138]Y. B. Bannett and I. Freund, *ibid.* 34, 372 (1975).
[139]P. Eisenberger, P. M. Platzman, and H. Winick, Phys. Rev. B13, 2377 (1976); Phys. Rev. Lett. 36, 623 (1976). P. M. Platzman and P. Eisenberger
[140]P. Nozieres and E. Abrahams, Phys. Rev. B10, 3099 (1974).
[141]S. A. Akhmanov, V. V. Fadeev, R. V. Khokhlov, and O. N. Chunaev, Pis'ma Zh. Eksp. Teor. Fiz. 6, 575 (1967) [JETP Lett. 6, 85 (1967)].
[142]D. N. Klyshko and D. P. Krindach, Zh. Eksp. Teor. Fiz. 54, 697 (1968) [Sov. Phys. JETP 27, 371 (1968)].
[143]D. Magde, R. Scarlet and H. Mahr, Appl. Phys. Lett. 11, 381 (1967).
[144]D. N. Klyshko, Pis'ma Zh. Eksp. Teor. Fiz. 6, 490 (1967) [JETP Lett. 6, 23 (1967)].
[145]D. N. Klyshko, Zh. Eksp. Teor. Fiz. 55, 1006 (1968) [Sov. Phys. JETP 28, 522 (1969)].
[146]D. A. Kleinman, Phys. Rev. 174, 1027 (1968).
[147]J. P. Budin, B. Godard, and J. Ducuing, IEEE J. Quantum Electron. QE-4, 831 (1968).
[148]T. G. Giallorenzi and C. L. Tang, Phys. Rev. 166, 225 (1968). H. J. Benson and D. L. Mills, *ibid.* B1, 4835 (1970). V. L. Strizhevskii and V. V. Obukhovskii, Zh. Eksp. Teor. Fiz. 58, 929 (1970) [Sov. Phys. JETP 31, 500 (1970)]; B. Ya. Zel'dovich, *ibid.*, 1348 [Sov. Phys. JETP 31, 723 (1970)]; V. M. Agranovich and V. L. Ginzburg, *ibid.* 61, 1243 (1971) [Sov. Phys. JETP 34, 662 (1972)].
[149]D. L. Weinberg, J. Appl. Phys. 41, 4239 (1970).
[150]N. Bloembergen and A. J. Sievers, Appl. Phys. Lett. 17, 483 (1970).
[151]S. Somekh and A. Yariv, *ibid.* 21, 140 (1972).
[152]Y. Yacoby, R. L. Aggarwal, and B. Lax, J. Appl. Phys. 44, 3180 (1973).
[153]I. Freund, Phys. Rev. Lett. 21, 1404 (1968). A. S. Chirkin, in Nelineinaya optika (Nonlinear Optics), "Nauka", Novosibirsk, 1968, p. 202.
[154]S. E. Harris *et al.*, IEEE J. Quantum Electron. QE-4, 354 (1968). G. D. Boyd, F. R. Nash, and D. F. Nelson, Phys. Rev. Lett. 24, 1298 (1970). D. N. Klyshko, N. I. Nazarova, and R. V. Khokhlov, Zh. Eksp. Teor. Fiz. 61, 1422 (1971) [Sov. Phys. JETP 34, 756 (1972)].
[155]I. Freund and B. F. Levine, Phys. Rev. Lett. 23, 854 (1969).
[156]I. Freund and B. F. Levine, Optics Comm. 3, 101 (1971).
[157]B. F. Levine and I. Freund, *ibid.* 1, 419 (1970).
[158]P. Eisenberger and S. L. McCall, Phys. Rev. Lett. 26, 684 (1971).
[159]B. F. Levine and I. Freund, Optics Comm. 3, 197 (1971).
[160]I. Freund and B. F. Levine, Phys. Lett. A31, 456 (1970).
[161]I. Freund and B. F. Levine, Phys. Rev. Lett. 25, 1241 (1970). I. Freund, Chem. Phys. Lett. 12, 583 (1972).
[162]P. M. Eisenberger and S. L. McCall, Phys. Rev. A3, 1145 (1971).
[163]J. W. F. Woo and S. S. Jha, *ibid.* B6, 4081 (1972).
[164]P. Eisenberger and S. L. McCall, IEEE J. Quantum Electron. QE-8, 522 (1972).
[165]S. S. Jha and J. W. F. Woo, Phys. Rev. B5, 4210 (1972); Nuovo Cimento B10, 229 (1972).
[166]I. Freund and B. F. Levine, Phys. Rev. B7, 4747; B8, 3059 (1973); Nuovo Cimento B20, 64 (1974).
[167]I. Freund, Optics Comm. 6, 421 (1972); Phys. Rev. A7, 1849 (1973). J. Eichler, *ibid.* A9, 1762 (1974).
[168]I. Freund, Optics Comm. 8, 401 (1973).
[169]I. V. Krasnov and N. Ya. Shaparev, Kvantovaya Elektron. (Moscow) 2, 2604 (1975) [Sov. J. Quantum Electron. 5, 1420 (1975)].
[170]S. A. Akhmanov and R. V. Khokhlov, Problemy nelineinoi optiki (Problems of Nonliner Optics), VINITI, M., 1964 (Engl. Transl., Gordon & Breach, New York, 1972); N. Blombergen, Nonlinear Optics, Benjamin, 1965,
[171]V. M. Fain, Kvantovaya radiofizika, t. 1. Fotony i nelineinye sredy (Quantum Radiophysics. Vol. 1. Photons and Nonlinear Media), Sov. radio, M., 1972.
[172]V. M. Agranovich and V. L. Ginzburg, Kristalooptika s uchetom prostranstvennoi dispersii i teoriya eksitonov (Crystal Optics with Account for Spatial Dispersion and the Theory of Excitons), Nauka, M., 1965 (Engl. Transl., Spatial Dispersion in Crystal Optics and the Theory of Excitons, Interscience, New York, 1966).
[173]V. A. Bushuev and D. N. Klyshko, Zh. Tekh. Fiz. 43, 2255 (1973) [Sov. Phys. Tech. Phys. 18, 1427 (1974)].
[174]V. M. Fain and E. G. Yashchin, Zh. Eksp. Teor. Fiz. 46, 695 (1964) [Sov. Phys. JETP 19, 474 (1964)]. P. N. Butcher and N. R. Ogg, Proc. Phys. Soc. 86, 699 (1965).
[175]M. L. Levine and S. M. Rytov, Teoriya ravnovesnykh teplovykh fluktuatsiĭ v elektrodinamike (Theory of Equilibrium Thermal Fluctuations in Electrodynamics), Nauka, M., 1967.
[176]Z. G. Pinsker, Dinamicheskoe rasseyanie rentgenovskikh

luchei v ideal'nykh kristallakh (Dynamical Scattering of X-Rays in Ideal Crystals), Nauka, M., 1974.
[177]A. S. Pine, Phys. Rev. **A139**, 901 (1965).
[178]V. A. Bushuev, Vestn. Moskovsk. un-ta, ser. III (Fizika, Astronomiya) **14**, No. 2, 177 (1973).
[179]V. A. Bushuev, *ibid.*, p. 735.
[180]V. A. Bushuev, Opt. Spektrosk. **36**, 355 (1974).
[181]V. A. Bushuev and R. N. Kuz'min, Zh. Tekh. Fiz. **44**, 2568 (1974) [Sov. Phys. Tech. Phys. **19**, 1590 (1975)].
[182]A. M. Afanasev, Yu. Kagan, and F. N. Chukhovskii, Phys. Stat. Sol. **28**, 287 (1968).
[183]F. N. Chukhovskiĭ, L. A. Alexanian, and Z. G. Pinsker, Acta Cryst. **A29**, 38 (1973).
[184]V. A. Bushuev and R. N. Kuz'min, in Proceedings of the Visiting Session of the Scientific Council of the Academy of Sciences of the USSR on the Problem "Formation and Structure of Crystals", Erevan State Univ. 1975, p. 101.
[185]H. J. Grenvill-Wells, Nature 168, 291 (1951). N. Norman, Acta Cryst. **11**, 1 (1958). Y. Yondeda, J. Phys. Soc. Japan 16, 1570 (1961). I. V. Telegina and E. V. Kolontsova, Kristallografiya 14, 603 (1969)].
[186]V. A. Bushuev, R. N. Kuz'min, and O. Yu. Tikhomirov, in Obrabotka i interpretatsiya fizicheskikh eksperimentov (Processing and Interpretation of Physical Experiments), No. 6, Moscow Univ. Press, 1977, p. 55.
[187]W. H. Zachariasen, Acta Cryst. 23, 558 (1967).
[188]M. N. Yakimenko, Usp. Fiz. Nauk **114**, 55 (1974) [Sov. Phys. Usp. 17, 651 (1975)].

Translated by M. V. King